INTERNATIONAL JOURNAL FOR NUMERICAL METHODS IN BIOMEDICAL ENGINEERING
Int. J. Numer. Meth. Biomed. Engng. (2015); e02755
Published online in Wiley Online Library (wileyonlinelibrary.com). DOI: 10.1002/cnm.2755

A guide to uncertainty quantification and sensitivity analysis for cardiovascular applications

Vinzenz Gregor Eck[1,‡], Wouter Paulus Donders[2,*,†,‡], Jacob Sturdy[1], Jonathan Feinberg[3,4], Tammo Delhaas[5], Leif Rune Hellevik[1,3] and Wouter Huberts[5]

[1]*Division of Biomechanics, Department of Structural Engineering, NTNU, Trondheim, Norway*
[2]*Department of Biomedical Engineering, School for Mental Health and Neuroscience, Maastricht University, Maastricht, The Netherlands*
[3]*Center for Biomedical Computing, Simula Research Laboratory, Lysaker, Norway*
[4]*Department of Mathematics, University of Oslo, Oslo, Norway*
[5]*Department of Biomedical Engineering, CARIM School for Cardiovascular Diseases, Maastricht University, Maastricht, The Netherlands*

SUMMARY

As we shift from population-based medicine towards a more precise patient-specific regime guided by predictions of verified and well-established cardiovascular models, an urgent question arises: *how sensitive are the model predictions to errors and uncertainties in the model inputs?* To make our models suitable for clinical decision-making, precise knowledge of prediction reliability is of paramount importance. Efficient and practical methods for uncertainty quantification (UQ) and sensitivity analysis (SA) are therefore essential. In this work, we explain the concepts of global UQ and global, variance-based SA along with two often-used methods that are applicable to any model without requiring model implementation changes: Monte Carlo (MC) and polynomial chaos (PC). Furthermore, we propose a guide for UQ and SA according to a six-step procedure and demonstrate it for two clinically relevant cardiovascular models: model-based estimation of the fractional flow reserve (FFR) and model-based estimation of the total arterial compliance (C_T). Both MC and PC produce identical results and may be used interchangeably to identify most significant model inputs with respect to uncertainty in model predictions of FFR and C_T. However, PC is more cost-efficient as it requires an order of magnitude fewer model evaluations than MC. Additionally, we demonstrate that targeted reduction of uncertainty in the most significant model inputs reduces the uncertainty in the model predictions efficiently. In conclusion, this article offers a practical guide to UQ and SA to help move the clinical application of mathematical models forward. Copyright © 2015 John Wiley & Sons, Ltd.

Received 16 June 2015; Revised 12 October 2015; Accepted 13 October 2015

KEY WORDS: uncertainty quantification; sensitivity analysis; cardiovascular modeling; Monte Carlo; polynomial chaos; fractional flow reserve; arterial compliance

1. INTRODUCTION

In the past decades, biomedical engineers have been applying physics-based mathematical models to unravel the complex cardiovascular system. These models relate all involved factors with physical and physiological laws. The resulting governing equations are solved by using advanced numerical techniques. Since then, great progress has been made in understanding cardiovascular (patho-)physiology [1–5]. Mathematical models have also been used to design and evaluate medical

*Correspondence to: Wouter Paulus Donders, Department of Biomedical Engineering, School for Mental Health and Neuroscience, Maastricht University, Maastricht, The Netherlands.
†E-mail: w.donders@maastrichtuniversity.nl
‡Authors contributed equally to the manuscript.

devices [6, 7], to develop training simulators for medical interventions [8], and to estimate model inputs that are impossible to measure directly [9]. More recently, engineers started aiming to apply these models for individualized diagnosis and intervention planning in the clinic [10, 11]. However, the translation of models from the pre-clinical phase to their use for patient-specific clinical decision-making is not straightforward. Although international initiatives like the Virtual Physiological Human (www.vph-institute.org) have made significant steps towards clinical application, personalized models (e.g., Digital Patient, www.digital-patient.net) are not yet routinely adopted in clinical practice.

One of the biggest challenges in the clinical application of models is the adaptation of model inputs to patient-specific conditions (model personalization). The inputs to be personalized may include the computational domain (e.g., vascular networks), physical parameters (e.g., vascular material properties), and boundary conditions (e.g., inflow and outflow conditions). All measurements of these inputs are hampered by measurement uncertainty (e.g., sphygmanometry [12]) as well as large biological variability (e.g., heart rate, mean blood pressure [13]), leading to uncertainties in the inputs. Furthermore, not all model inputs are directly (or indirectly) measurable (e.g., local mechanical properties of the arterial wall) and if they are, the measurements may be costly (e.g., when MRI is the only available modality).

A second challenge is to determine the level of model complexity that yields the most accurate outcome measure. Model complexity is increased when the model more accurately describes reality (e.g., by using more detailed computational domains or including physiological processes such as regulation). This reduces the uncertainty in the model output because of the model framework. However, this simultaneously increases the uncertainty in the model output because more model inputs must be assessed patient-specifically. Hence, an optimal trade-off must be found between the uncertainty resulting from the model framework and the uncertainty resulting from (measured) model inputs that lead to a minimal total uncertainty (Figure 1). To tackle these challenges, it is crucial to quantify the uncertainty in the model output(s) that results from uncertainties in model inputs. In addition, it is necessary to identify which model inputs can be fixed to population-based values (input fixing) and which are most rewarding to measure accurately (input prioritization). Therefore, proper uncertainty quantification (UQ) and sensitivity analysis (SA) are indispensable.

The available methods for UQ and SA can roughly be divided into local methods and global methods. Local methods examine the effect on the output of an infinitesimal change around a reference value of one model input while keeping all others fixed. Thus, only information that is local to the reference value is obtained. In clinical applications of cardiovascular models, the uncertainties in model inputs are relatively large. The dependency of the model output on the input may be non-additive, non-monotonic, and non-linear in some locations of the input space (for example, see Figure 2). If that is the case, the results from local methods will be misleading. Therefore, they should be discarded in favor of global methods which *do* consider the whole input space and which can account for non-additive, non-monotonic, and non-linear dependencies of the output on the input.

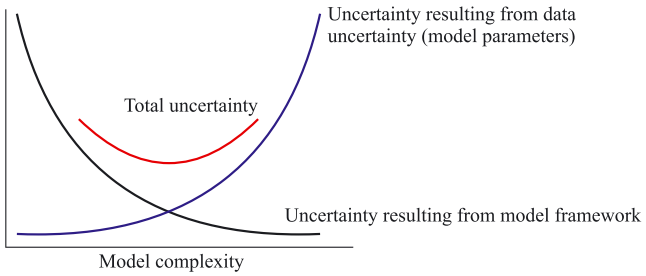

Figure 1. The trade-off between increasing model complexity and decreasing the number of uncertain inputs. Figure was reprinted from Huberts *et al.* [14].

DOI: 10.1002/cnm

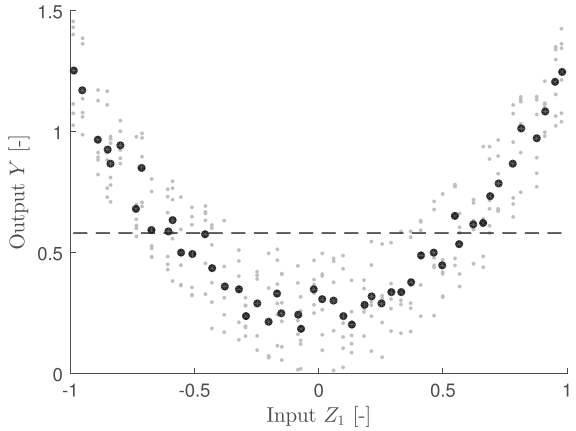

Figure 2. Example of non-linear, non-monotonic model output behavior for a model with interacting model inputs, Z_1 and Z_2. The gray bullets (•) correspond to outputs $Y = f(Z_1, Z_2)$ (plotted as (Z_1, Y) with the values of Z_2 implicitly varying along an orthogonal axis), whereas the black bullets (•) indicate the expected value of Y for fixed values of Z_1, that is, $\mathbb{E}[Y \mid Z_1]$.

Global methods can be categorized into intrusive and non-intrusive methods. In the intrusive approaches, a parameterization of the uncertainty in the model inputs is substituted into the model to derive new governing equations. The new governing equations are then solved using particular numerical schemes. Intrusive approaches can be very complex and hard to implement. Examples of intrusive global methods are the perturbation method [15, 16], the moment equation approach [17], and the stochastic spectral Galerkin method (an intrusive polynomial chaos (PC) method) [18, 19].

On the other hand, non-intrusive methods do not require changes to the numerical code of existing models. Instead, model outcomes are obtained using the deterministic solver for a set of different input samples. UQ and SA are then performed on the obtained output realizations. This approach can be applied for any model with any numerical implementation, and it is therefore much better suited to achieve model personalization of existing cardiovascular models. Examples of non-intrusive global methods are the Monte Carlo (MC) method [20], the PC method [21, 22], and the Lagrangian interpolation method [23, 24].

Although the importance of UQ and SA for patient-specific cardiovascular modeling is widely recognized, the number of papers that apply global UQ or SA is very small with respect to the number of papers describing cardiovascular models aiming for clinical decision-making (we identified papers with global methods in [5, 25–34]). A possible explanation for this might be that the translation of mathematical models for clinical decision-making is still in its infancy. In addition, it is possible that biomedical engineers are not aware of the available global UQ and SA methods that are used outside their own field of expertise. Finally, the commonly high computational cost of global methods might explain the limited number of papers that apply UQ and SA within the biomedical engineering community.

Because we strongly believe that UQ and SA are essential tools in taking the next step to make mathematical models suitable for clinical decision-making, we will give an overview of available non-intrusive UQ and SA methods that are most often applied outside our own field (e.g., reliability engineering). In particular, we focus on the non-intrusive MC and PC methods and present an overview of the methods, the mathematical ideas behind, and their application for UQ and SA. In addition, we provide a guide on how to apply these methods with two examples.

This article is outlined as follows. In Section 2, some basic definitions used later on are described. Common uncertainty and sensitivity measures will be introduced in Section 3 and 4, respectively. In Sections 5 and 6, we will give an overview of the MC and PC methods used for non-intrusively deriving the measures for uncertainty and sensitivity. In Section 7, we present a general procedure for non-intrusive MC and PC. In addition, we demonstrate both methods using two examples with clinical relevance. The first example considers a model to estimate the fractional flow reserve

DOI: 10.1002/cnm

(Section 7.3). The second example considers a model to estimate total arterial compliance using the pulse-pressure method (Section 7.4). Finally, we discuss the advantages, disadvantages, and limitations of the discussed methods in Section 8.

2. DEFINITIONS

In the following, we introduce briefly the black box representation for a patient-generic mathematical model and some concepts of probability theory needed to understand the applied methods. We recommend Gardiner [35] or Xiu [36] for more information about the basic concepts of probability theory.

We regard a patient-generic mathematical model represented by a (functional) black box f:

$$y = f(\mathbf{z}), \tag{1}$$

where y is the *deterministic* output of interest for the *deterministic* inputs $\mathbf{z} = [z_1, z_2, \ldots, z_D]$. For the ease of notation, we assume y to be a scalar value (i.e., a single output of interest), although y may be in general a vector of different quantities over space and time.

The inputs of the model are subjected to uncertainty, as they may not be assessed accurately (if at all) or because they may reflect biological parameters that vary over short time periods (e.g., the variation of heart rate over the day [13]). As a result, the output is uncertain as well, and therefore, we write (1) as a black box model with a *stochastic* output Y and *stochastic* inputs $\mathbf{Z} = [Z_1, Z_2, \ldots, Z_D]$:

$$Y = f(\mathbf{Z}). \tag{2}$$

The inputs $\mathbf{Z}$ may be material/geometric parameter values (e.g., aortic diameters, stroke volume, and heart rate), boundary conditions, and initial conditions (e.g., arterial flow). The output of interest Y may be, for example, the fractional flow reserve (FFR) or the total arterial compliance C_T (see also examples in Section 7).

To account for the uncertainty in Z_i, we consider each Z_i, $i = 1, 2, \ldots, D$ to be defined as a continuous random variable[‡]. Z_i can take any value z_i in its sample space Ω_i. The likelihood that a certain value z_i is drawn from the sample space for $\mathbf{Z}_i$ is defined by the probability density function ρ_i. Integrating ρ_i over a domain $[a, b] \subset \Omega_i$ yields the probability P that Z_i takes a value z_i in $[a, b]$:

$$\mathrm{P}(a \leqslant Z_i \leqslant b) = \int_a^b \rho_i(z)\,\mathrm{d}z. \tag{3}$$

An uncertain input Z_i is commonly defined as a uniform, normal, or chi-squared random variable depending on the available information (i.e., a random variable with the corresponding probability density function).

The uncertain input vector $\mathbf{Z}$ is defined as a (multivariate) random variable, that is, a random variable consisting of other random variables, namely, all $Z_i, i = 1, 2, \ldots, D$ with the sample space $\Omega_\mathbf{Z} = \Omega_1 \times \Omega_2 \times \cdots \times \Omega_D$. The likelihood that a set of specific values (samples) $\mathbf{z}$ in $\Omega_\mathbf{Z}$ is drawn for the uncertain input vector $\mathbf{Z}$ is given by the joint probability distribution $\rho_\mathbf{Z}$. The stochastic methods applied in this article, in particular the polynomial chaos method and the Sobol variance decomposition, require that the uncertain inputs Z_i are independent; hence, the joint distribution density function $\rho_\mathbf{Z}$ is given by

$$\rho_\mathbf{Z}(\mathbf{z}) = \prod_{i=1}^{D} \rho_i(z_i). \tag{4}$$

[‡]Cardiovascular models usually have continuous inputs. However, the methods discussed in the article are also sufficiently general to allow for discrete random variables.

DOI: 10.1002/cnm

The assessment of the uncertain input distributions is an integral part of the UQ and SA procedure; however, it is generally very problem-specific and as such we give only a brief introduction and recommend further reading in the proposed literature. In general, the input distribution is either elicited from experts or estimated from patient-specific measurements. For an introduction to expert elicitation, take a look at the work of O'Hagen [37]. If detailed patient-specific measurements are available, a density function can be estimated using Bayesian inference [38]. Commonly, at least of expert elicitation, the resulting density functions are normal and uniform. In the second example (Section 7.4), we demonstrate how the distributions of the random input can be assessed from population-based data and data literature. If the random input is characterized by a high-dimensional and infinite-dimensional processes, respectively, principal component analysis [39] or Karhunen–Loeve expansion [36] may be applied.

The output of interest Y is also considered a random variable with an associated probability density function ρ_Y. The density function ρ_Y is dependent on $\mathbf{Z}$, which is governed by the model f. It is useful to know the distribution of ρ_Y, for example, to be able to assess the uncertainty of Y. In general, it is quite cumbersome or even impossible to derive an analytic expression for ρ_Y because f is complex (i.e., highly non-linear and/or interacting terms) and has no analytic solution. However, with the MC method (Section 5) and the generalized PC method (Section 6), it is possible to obtain useful characteristics of ρ_Y using methods of uncertainty quantification (Section 3). Moreover, a global, variance-based sensitivity analysis is able to apportion the uncertainty of Y to particular uncertain inputs and groups of interacting uncertain inputs (Section 4).

3. UNCERTAINTY QUANTIFICATION

The aim of UQ is to describe the unknown distribution of the stochastic model f with output Y that arises from the uncertain inputs $\mathbf{Z}$, that is, to obtain useful metrics to describe ρ_Y. We briefly review statistical moments, percentiles, and confidence intervals as useful metrics for UQ (see also, e.g., [35]).

3.1. Statistical moments

Many uncertainty measures are based upon statistical moments. The two most common are expected value and variance. The expected value, also known as the first moment of Y and mean, is defined as

$$\mu[Y] = \mathbb{E}[Y] = \int_{\Omega_Y} y\rho_Y(y)\,\mathrm{d}y. \tag{5}$$

The value of $\mathbb{E}[Y]$ is the center of the probability density mass and represents the expected output of the model f for multiple samples of $\mathbf{z}$ as the number of samples of $\mathbf{z}$ goes to infinity (see also Figures 3 and 6). The variance, also known as the second moment of Y, is defined as

$$\mathbb{V}[Y] = \int_{\Omega_Y} (y - \mathbb{E}[Y])^2 \rho_Y(y)\mathrm{d}y. \tag{6}$$

The variance is a measure of how much we should expect the output Y to deviate from the mean. It is conventionally used as a measure of uncertainty (see also Figures 3 and 6). The standard deviation is related to the variance by

$$\sigma[Y] = \sqrt{\mathbb{V}[Y]}, \tag{7}$$

which is easier to interpret because it has the same units as Y.

3.2. Percentiles and prediction intervals

The x-th percentile of Y is the value of Y under which $x\%$ of observations/realizations of Y are located. For example, the 50-th percentile is the median, which can be used as an alternative to the

DOI: 10.1002/cnm

mean (although they are generally not the same value). Generally, the $(\beta \cdot 100)$-th percentile $y_{[\beta]}$ is the value under which $(\beta \cdot 100)\%$ of the observations of Y fall:

$$\beta = \int_{-\infty}^{y_{[\beta]}} \rho_Y(y)\mathrm{d}y. \tag{8}$$

Percentiles can be used to define prediction intervals[§]. A $(\beta \cdot 100)\%$ prediction interval I_β is a range of values $[y_l, y_h]$ such that the probability of finding a value y outside this range (i.e., $y < y_l$ or $y > y_h$) is $(\beta \cdot 50)\%$ at each side:

$$I_\beta = \left[y_{[\beta/2]}, y_{[1-\beta/2]}\right]. \tag{9}$$

These intervals may thus be used to estimate finite bounds where the value of Y is expected to be with a margin of error equal to $(\beta \cdot 100)\%$. The value of β therefore represents the trade-off between the error margin and the size of the interval. Prediction intervals are useful for limiting the range of a variable Y.

Another use of the percentile measure is to create visual representation densities through histograms. Histograms can be created by finding percentiles over a set of intervals. The histogram is an approximation ρ_Y and mostly used to visualize the probability density function (e.g., Figures 3 and 6).

4. SENSITIVITY ANALYSIS

The aim of SA is to quantify the contribution to the output Y of particular uncertain inputs Z_i and their interactions. As the behavior of the output with respect to the input (e.g., linearity, monotonicity, and additivity) is generally not known beforehand, a method is desired that does not make any assumptions about it. A global, variance-based SA is applicable for all models and can be used to quantify the portions of the total output variance that are contributed by each model input and their interactions. This is useful for model personalization, for which there are two specific goals: identifying uncertain inputs Z_i that have little or no effect on the output Y by itself or through interaction (input fixing) and quantifying the expected reduction in the output uncertainty if an uncertain input Z_i were known exactly (input prioritization). Sobol introduced global, variance-based sensitivity indices that can be used to achieve both goals. These indices are defined and explain in the following section. For mathematical details, we refer to the literature [41, 42] and Appendix A.

4.1. First and second-order sensitivity indices

The term $\mathbb{E}[Y \mid Z_i]$ is the conditional expectation and represents the expected value of the output Y for a fixed value of the uncertain input Z_i [35]. The direct effect of Z_i is given by the first-order Sobol sensitivity index, which is also called the main sensitivity index. It is defined by

$$S_i = \frac{\mathbb{V}[\mathbb{E}[Y \mid Z_i]]}{\mathbb{V}[Y]}, \tag{10}$$

where $1 \leqslant i \leqslant D$. The main index S_i quantifies the portion that Z_i contributes directly (without interaction) to the total variance $\mathbb{V}[Y]$. More specifically, S_i is the expected reduction in $\mathbb{V}[Y]$ that can be achieved if Z_i would be fixed on its unknown true value. Therefore, the main sensitivity index is useful for determining which uncertain inputs should be assessed more precisely (i.e., input prioritization) [43].

The second-order sensitivity indices represent the portion of the total variance $\mathbb{V}[Y]$ that results solely from the interaction between Z_i and Z_j. They are defined as

[§]Note that in statistics, there are three different types of intervals: credible, confidence, and prediction intervals with some overlapping definition [40]. We here use prediction intervals as intervals related to estimation of values in the future.

DOI: 10.1002/cnm

$$S_{ij} = \frac{\mathbb{V}\left[\mathbb{E}\left[Y \mid Z_i, Z_j\right]\right]}{\mathbb{V}[Y]}. \tag{11}$$

Higher-order sensitivity indices also exist and may be calculated analogously to (11) [43]. The number of higher-order sensitivity indices is $2^D - D - 1$ and is therefore usually not estimated in practice.

4.2. Total sensitivity indices

To consider interaction effects without the need to estimate all higher-order sensitivity indices, Homma and Saltelli introduced the total sensitivity index, which is the sum of all first and higher-order effects where Z_i is involved [44]. The total sensitivity index of Z_i is given by

$$S_{\mathrm{T},i} = \frac{\mathbb{V}[Y] - \mathbb{V}\left[\mathbb{E}\left[Y \mid Z_{-i}\right]\right]}{\mathbb{V}[Y]} = 1 - \frac{\mathbb{V}\left[\mathbb{E}\left[Y \mid Z_{-i}\right]\right]}{\mathbb{V}[Y]}, \tag{12}$$

where Z_{-i} is the set of all uncertain inputs except Z_i. The total sensitivity index, $S_{\mathrm{T},i}$, represents the total variance attributable both to the direct effect and all interaction effects of input Z_i (see also Figures 4 and 7). The difference $S_{\mathrm{T},i}$–S_i represents the accumulation of all higher-order interactions, where the minimum of zero indicates no interactions are present. Because the total sensitivity index considers not only the direct effect but also all others effects in which an input is involved, it is useful for determining which uncertain inputs can be fixed within their uncertainty domain (i.e., input fixing), as they are not important when $S_{\mathrm{T},i}$ is close to zero.

Example: Consider $D = 3$ inputs with the following sensitivities: $S_1 = 0.02$, $S_2 = 0.13$, $S_3 = 0.53$, $S_{12} = 0.0$, $S_{13} = 0.03$, $S_{23} = 0.27$, $S_{123} = 0.01$. The total sensitivity indices are therefore $S_{\mathrm{T},1} = S_1 + S_{12} + S_{13} + S_{123} = 0.07$, $S_{\mathrm{T},2} = S_2 + S_{12} + S_{23} + S_{123} = 0.41$ and $S_{\mathrm{T},3} = S_3 + S_{13} + S_{23} + S_{123} = 0.84$. The main sensitivities and total sensitivities are summarized in Table I. By considering the main sensitivity indices, it can be concluded that it is most rewarding to measure input 3 more accurately because it has the highest main sensitivity index. If input 3 could be fixed to its true value, 53% of the output uncertainty would be reduced. Considering the total sensitivity indices, it can be concluded that fixing both inputs 2 and 3 would leave just 7% of the current output uncertainty. Input 1 could therefore be fixed within its uncertainty domain.

5. MONTE CARLO METHOD

The uncertainty measures and sensitivity measures described in Sections 3 and 4 can be estimated using numerical methods. MC simulation is most commonly applied for this task because of its simplicity and wide-ranging applicability. MC simulations consists of three basic steps:

1. Use a sampling method to draw a set of input samples $\left\{\mathbf{z}^{(s)}\right\}_{s=1}^{N_\mathrm{s}}$ from the input space $\Omega_\mathbf{Z}$ that is defined by the joint probability density function $\rho_\mathbf{Z}$.
2. Evaluate the deterministic model $f(\mathbf{z})$ for each sample in $\left\{\mathbf{z}^{(s)}\right\}_{s=1}^{N_\mathrm{s}}$ to realize a set of outputs of interests $\left\{\boldsymbol{y}^{(s)}\right\}_{s=1}^{N_\mathrm{s}}$. (Note, $\left\{\boldsymbol{y}^{(s)}\right\}_{s=1}^{N_\mathrm{s}}$ are effectively randomly sampled from ρ_Y.)
3. Estimate all uncertainty measures and sensitivity indices directly from $\left\{\boldsymbol{y}^{(s)}\right\}_{s=1}^{N_\mathrm{s}}$.

The basic method can be implemented with only a few lines of code using any programming language that supports (pseudo-)random number generation.

Table I. The main and total sensitivity indices for the example case in Section 4.

	$i = 1$	$i = 2$	$i = 3$
Main (S_i)	0.02	0.13	0.53
Total ($S_{\mathrm{T},i}$)	0.07	0.41	0.84

DOI: 10.1002/cnm

The asymptotic approximation error for any measure calculated with the MC method using random sampling is $\sigma_Y / \sqrt{N_s}$ [20], which means that the convergence rate is completely independent of the number of dimensions D. However, the number of evaluations required to achieve an acceptable error can be astronomical in part because the asymptotic error estimate may only be valid for very large values of N_s. Thus, if evaluation of the model function f is computational costly, achieving reasonably accurate estimates of the uncertainty measures and sensitivity indices may be infeasible. The convergence rate may be improved by drawing samples using alternative sample schemes. Such alternative sample schemes prevent clustering of samples and ensure that samples fully cover the input space [45]. Examples of this include Latin hypercube sampling [46] and quasi-random sampling [45]. In the latter case, samples are constructed from deterministic Halton, Sobol, or Fauré sequences [47, 48]. For more information on MC, we refer the interested reader to [20, 49, 50]. Software toolboxes that support quasi-random sampling and Latin hypercube sampling can be found in, for example, [Python] `Chaospy` [51], `Dakota` [52], [Scilab] `NISP` [53], [MATLAB] `SAFE` [54], and [R] `Sensitivity` [55].

5.1. Uncertainty quantification

The expected value μ_Y defined in (5) can be estimated from the evaluations of Y as follows:

$$\mathbb{E}[Y] \approx \mathbb{E}_{\mathrm{MC}}[Y] = \frac{1}{N_s} \sum_{s=1}^{N_s} y^{(s)}. \tag{13}$$

Likewise, the variance in (6) can be estimated as

$$\mathbb{V}[Y] \approx \mathbb{V}_{\mathrm{MC}}[Y] = \frac{1}{N_s - 1} \sum_{s=1}^{N_s} \left(y^{(s)} - \mathbb{E}_{\mathrm{MC}}[Y] \right)^2. \tag{14}$$

Prediction intervals as defined in (9) are easily estimated by first sorting the evaluations $y^{(s)}, s = 1, 2, \ldots, N_s$ in increasing order, that is, re-index the evaluations $y^{(s)}$ as $y'^{(s)}$ such that $y'^{(1)} \leqslant y'^{(2)} \leqslant \cdots \leqslant y'^{(N_s)}$. Using this reordering, the values corresponding to the desired percentiles $(\beta 100/2)$ and $(100 - \beta 100/2)\%$ as defined in (9) are estimated as

$$I_\beta \approx \left[y'^{(N_s \beta/2)}, y'^{(N_s(1-\beta/2))} \right]. \tag{15}$$

Note that if $N_s \beta$ is not an integer, the percentile may be calculated using linear interpolation between $y'^{(\lfloor N_s \beta/2 \rfloor)}$ and $y'^{(\lceil N_s \beta/2 \rceil)}$. Alternatives to this method may be found in [56].

5.2. Sensitivity analysis

Straightforwardly applying the MC method to estimate the main and total sensitivity indices defined in (10) and (12) requires an inner and outer loop of integral evaluations. Let N be the number of samples used to evaluate an integral using MC to some accuracy. Then, a straightforward MC approach would require $2DN^2$ evaluation for a full set of main and total sensitivity indices. To improve the convergence rate, Saltelli devised an alternative MC procedure to obtain a full set of main and total sensitivity indices, which reduces the total number of model evaluations from $N_s = 2DN^2$ to $N_s = N(D + 2)$ [44, 57]. Similar procedures for the main and total sensitivity indices have been proposed by Saltelli *et al.* [58], Jansen [59], Sobol *et al.* [60], and Homma [44]. An overview comparing these different procedures in terms of accuracy can be found in the work of Saltelli *et al.* [58]. Implementations of these procedures can be found in, for example, `Dakota` [52], [Scilab] `NISP` [53], [MATLAB] `SAFE` [54], [Python] `SALib` [61], and [R] `sensitivity` [55].

We now present Saltelli's efficient numerical procedure to estimate the main and total sensitivity indices as presented in [57]. The first step of the Saltelli method is to create two independent sampling matrices:

DOI: 10.1002/cnm

$$\mathbf{A} = \begin{bmatrix} z_1^{(1)} & z_2^{(1)} & \cdots & z_D^{(1)} \\ z_1^{(2)} & z_2^{(2)} & \cdots & z_D^{(2)} \\ \vdots & \vdots & \ddots & \vdots \\ z_1^{(N)} & z_2^{(N)} & \cdots & z_D^{(N)} \end{bmatrix} \quad \mathbf{B} = \begin{bmatrix} z_1'^{(1)} & z_2'^{(1)} & \cdots & z_D'^{(1)} \\ z_1'^{(2)} & z_2'^{(2)} & \cdots & z_D'^{(2)} \\ \vdots & \vdots & \ddots & \vdots \\ z_1'^{(N)} & z_2'^{(N)} & \cdots & z_D'^{(N)} \end{bmatrix}. \tag{16}$$

The matrix $\mathbf{A}$ contains N samples $\mathbf{z}^{(s)} = [z_1^{(s)}, z_2^{(s)}, \ldots, z_D^{(s)}]$, whereas the matrix $\mathbf{B}$ contains N samples $\mathbf{z}'^{(s)} = [z_1'^{(s)}, z_2'^{(s)}, \ldots, z_D'^{(s)}]$. The samples of $\mathbf{A}$ and $\mathbf{B}$ are drawn independently of each other.

As a second step, D matrices $\mathbf{C}_i$, $i = 1, 2, \ldots, D$ are generated from matrices $\mathbf{A}$ and $\mathbf{B}$, where all columns are taken from $\mathbf{B}$ except for the i-th column, which is taken from $\mathbf{A}$:

$$\mathbf{C}_i = \begin{bmatrix} z_1'^{(1)} & \cdots & z_{i-1}'^{(1)} & z_i^{(1)} & z_{i+1}'^{(1)} & \cdots & z_D'^{(1)} \\ z_1'^{(2)} & \cdots & z_{i-1}'^{(2)} & z_i^{(2)} & z_{i+1}'^{(2)} & \cdots & z_D'^{(2)} \\ \vdots & \ddots & \vdots & \vdots & \vdots & \ddots & \vdots \\ z_1'^{(N)} & \cdots & z_{i-1}'^{(N)} & z_i^{(N)} & z_{i+1}'^{(N)} & \cdots & z_D'^{(N)} \end{bmatrix}. \tag{17}$$

The third step of Saltelli's procedure is to calculate the model evaluations for each row in all sample matrices, denoted as $y_{\mathrm{A}}^{(s)} = f(\mathbf{A}^{(s)})$, $y_{\mathrm{B}}^{(s)} = f(\mathbf{B}^{(s)})$, and $y_{\mathrm{C}_i}^{(s)} = f(\mathbf{C}_i^{(s)})$, where the superscript s denotes the s^{th} row of $\mathbf{A}$, $\mathbf{B}$, and $\mathbf{C}_i$, respectively.

5.2.1. Main sensitivity indices. The main sensitivity indices are estimated as

$$S_i \approx \frac{U_i - \mathbb{E}_{\mathrm{MC}}[Y]^2}{\mathbb{V}_{\mathrm{MC}}[Y]}, \tag{18}$$

with

$$U_i = \frac{1}{N-1} \sum_{s=1}^{N} y_{\mathrm{A}}^{(s)} y_{\mathrm{C}_i}^{(s)}. \tag{19}$$

The square of the expected value and the total variance in Equation (18) are estimated as proposed in [57]:

$$\mathbb{E}_{\mathrm{MC}}[Y]^2 = \frac{1}{N} \sum_{s=1}^{N} y_{\mathrm{A}}^{(s)} y_{\mathrm{B}}^{(s)}, \quad \mathbb{V}_{\mathrm{MC}}[Y] = \frac{1}{N-1} \sum_{s=1}^{N} \left(y_{\mathrm{B}}^{(s)} \right)^2 - \mathbb{E}_{\mathrm{MC}}[Y]^2. \tag{20}$$

5.2.2. Total sensitivity indices. The total sensitivity indices are estimated as

$$S_{\mathrm{T},i} \approx \frac{U_i' - \mathbb{E}_{\mathrm{MC}}[Y]^2}{\mathbb{V}_{\mathrm{MC}}[Y]}, \tag{21}$$

where

$$U_i' = \frac{1}{N-1} \sum_{s=1}^{N} y_{\mathrm{B}}^{(s)} y_{\mathrm{C}_i}^{(s)}. \tag{22}$$

The square of the expected value and the total variance in Equation (21) are estimated as proposed in [57]:

$$\mathbb{E}_{\mathrm{MC}}[Y]^2 \approx \left(\frac{1}{N} \sum_{s=1}^{N} y_{\mathrm{A}}^{(s)} \right)^2, \quad \mathbb{V}_{\mathrm{MC}}[Y] = \frac{1}{N-1} \sum_{s=1}^{N} \left(y_{\mathrm{A}}^{(s)} \right)^2 - \mathbb{E}_{\mathrm{MC}}[Y]^2. \tag{23}$$

DOI: 10.1002/cnm

6. POLYNOMIAL CHAOS METHOD

Another method to approximate the uncertainty and sensitivity measures is the PC method[¶]. In this method, a model output Y is expanded into a series of orthogonal polynomials, which are functions of the uncertain inputs $\mathbf{Z}$ [19, 62]. The orthogonal polynomials are basis functions that span the output space of Y. The PC method results in an analytic expression, that is, the PC expansion, from which the statistical moments and variance-based sensitivity indices can be calculated analytically. The PC expansion is expressed in terms of the orthogonal polynomials and expansion coefficients, which can already be obtained with a relatively low number of input samples [19, 21, 22].

The PC method is a competitive alternative to the MC method for UQ and SA. However, the PC method is not as easy to implement as MC. It is therefore recommended to use a software toolkit that has already implemented the PC method. Various implementations for different programming environments are as follows: [Python] `Chaospy` [51], `Dakota` [52], [C++] `MITUQ` [63], [Scilab] `NISP` [53], [Python] `OpenTurns` [64], and [C++] `UQToolkit` [65].

In this section, we briefly describe the construction of a PC expansion and the most common methods for obtaining the expansion coefficients. Furthermore, we outline the calculations of the uncertainty measures: $\mathbb{E}[Y]$ (5), $\mathbb{V}[Y]$ (6) and prediction intervals (9) in addition to sensitivity measures S_i (10) and $S_{\mathrm{T},i}$ (12).

6.1. Construction of a polynomial chaos expansion

Two equivalent, generalized expressions for a truncated polynomial chaos expansion[‖] of an output Y can be found in the literature [14, 21, 22, 66]:

$$Y \approx f_{\mathrm{PC}}(\mathbf{Z}) = \begin{cases} \displaystyle\sum_{e=0}^{N_{\mathrm{p}}-1} c_e \Phi_e(\mathbf{Z}), \\ \displaystyle\sum_{\boldsymbol{\alpha}\in\mathcal{A}} c_{\boldsymbol{\alpha}} \Phi_{\boldsymbol{\alpha}}(\mathbf{Z}). \end{cases} \tag{24}$$

In (24), c are the expansion coefficients, Φ are the polynomials, $\boldsymbol{\alpha} = (\alpha_1, \alpha_2, \ldots, \alpha_D)$ are multi-indices with nonzero entries, and $\mathcal{A}$ is the set of $N_{\mathrm{p}} = \binom{D+p}{p}$ multi-indices $\boldsymbol{\alpha}$ for all polynomials with a maximal order p. The same polynomials are also represented with an integer index e, which has a one-to-one relationship with $\boldsymbol{\alpha}$. The two alternative representations of the same polynomials will be used interchangeably.

Example: if $D = 3$, the first few polynomials ($\Phi_e \equiv \Phi_{\boldsymbol{\alpha}}$) are

$$\Phi_0 \equiv \Phi_{(0,0,0)}, \Phi_1 \equiv \Phi_{(1,0,0)}, \Phi_2 \equiv \Phi_{(0,1,0)}, \Phi_3 \equiv \Phi_{(0,0,1)}, \text{etc.}$$

The multi-indices $\boldsymbol{\alpha}$ can be used to construct Φ from univariate polynomials $\phi(Z_i)$ with tensor products:

$$\Phi_{\boldsymbol{\alpha}}(\mathbf{Z}) = \prod_{i=1}^{D} \phi_{\alpha_i}(Z_i), \tag{25}$$

where ϕ_{α_i} is a univariate polynomial of order α_i. The type of univariate polynomial ϕ_{α_i} is determined by the distribution of input Z_i according to the Wiener–Askey scheme [19]. For example, Hermite polynomials are recommended if the input distribution ρ_i of Z_i is Gaussian, whereas Legendre polynomials are used if ρ_i is uniform. The complete Wiener–Askey scheme can be found

[¶]Originally, the PC method was based on Hermite polynomials [62]. The method was later extended to handle different types of orthogonal polynomials by Xiu and Karniadakis [19] and consequently renamed to *generalized Polynomial Chaos method*. However, for the ease of notation, we will refer to the method with *PC*.

[‖]Further information on truncation and truncating methods can be found in [67, 68].

DOI: 10.1002/cnm

in Appendix B. The expected value of each Φ_e, $e = 1, 2, \ldots, N_\mathrm{p} - 1$, is zero for multivariate polynomials constructed from univariate polynomials in the Wiener–Askey scheme:

$$\mathbb{E}[\Phi_e] = \int_{\Omega_\mathbf{Z}} \Phi_e(\mathbf{z}) \rho_\mathbf{Z}(\mathbf{z})\, \mathrm{d}Z_i = 0, \tag{26}$$

and one for $e = 0$ because $\Phi_0 = 1$. The orthogonality of the multivariate polynomials follows from the property that

$$\int_{\Omega_\mathbf{Z}} \Phi_i(\mathbf{z}) \Phi_j(\mathbf{z}) \rho_\mathbf{Z}(\mathbf{z}) \mathrm{d}\mathbf{z} = \Delta_{ij} H_i, \tag{27}$$

where Δ_{ij} is the Kronecker delta and the term H_i is the normalization factor associated with the polynomial Φ_i (see also Appendix B). Analytical expressions for the normalization factors can be obtained from the literature [19, 69].

6.2. *Estimation of the expansion coefficients*

The polynomial chaos expansion in (24) is a general expression that can be used for any model output. The value of the expansion coefficients make the expansion specific to a particular output. There are two common approaches to obtain the expansion coefficients c non-intrusively: spectral projection and regression. The spectral projection approach exploits the orthogonality of the polynomials and requires a numerical integration for which specific input samples must be used. The regression approach minimizes a difference between the model outcome and the value of the polynomial expansion for input samples.

6.2.1. Spectral projection. In the projection approach (also called *the pseudo-spectral approach* and *discrete projection*), each expansion coefficient $c_{\boldsymbol{\alpha}}$ is estimated by projecting the solution onto the space spanned by the orthogonal polynomials with the inner product. This is analogous to the calculation of the Fourier coefficients in the approximation of an arbitrary periodic function. Exploitation of the orthogonality property (27) yields

$$c_{\boldsymbol{\alpha}} = \frac{1}{H_{\boldsymbol{\alpha}}} \int_{\Omega_\mathbf{Z}} f(\mathbf{z}) \Phi_{\boldsymbol{\alpha}}(\mathbf{z}) \rho_\mathbf{Z}(\mathbf{z}) \mathrm{d}\mathbf{z}. \tag{28}$$

A numerical integration method can be used to approximate the integral. Good approximations can be achieved with tensor or sparse grid quadrature because the integrands are smooth polynomials [70]. The expansion coefficients from (28) are then approximated by a discrete sum:

$$c_{\boldsymbol{\alpha}} \approx \frac{1}{H_{\boldsymbol{\alpha}}} \sum_{s=1}^{N_\mathrm{s}} f(\mathbf{z}^{(s)}) \Phi_{\boldsymbol{\alpha}}(\mathbf{z}^{(s)}) w_s. \tag{29}$$

Here, each sample $\mathbf{z}^{(s)}$ has a weight w_s as determined by the used tensor quadrature or sparse grid quadrature.

When using tensored quadrature, the number of samples is given by $N_\mathrm{s} = (N_\mathrm{1D})^D$, where N_1D is the number of nodes in the one-dimensional quadrature rule. For large D, the number of samples N_s becomes large (the 'curse of dimensionality'). Sparse grids quadratures are constructed from one-dimensional quadrature rules using Smolyak's algorithm [71, 72]. The total number of samples N_s in the sparse grid are less than the tensored quadrature when using the same one-dimensional rule, but an additional approximation error is introduced (for specific approximation error bounds, see [73, 74]).

6.2.2. Regression. The regression method minimizes a normed difference between the PC expansion and the output for a set of samples, i.e. it solves the minimization problem:

$$\arg\min_{\vec{c}} \left\| f(\mathbf{Z}) - \sum_{e=0}^{N_\mathrm{p}-1} c_e \Phi_e(\mathbf{Z}) \right\|, \tag{30}$$

DOI: 10.1002/cnm

where any L^q-norm $\|(\cdot)\|_q = (\sum(\cdot)^q)^{\frac{1}{q}}$ can be used. Often, the L^2-norm is used, which reduces (30) to the following linear least squares problem [21]:

$$\underbrace{\begin{bmatrix} \Phi_0\left(\mathbf{z}^{(1)}\right) & \Phi_1\left(\mathbf{z}^{(1)}\right) & \dots & \Phi_{N_\mathrm{p}-1}\left(\mathbf{z}^{(1)}\right) \\ \Phi_0\left(\mathbf{z}^{(2)}\right) & \Phi_1\left(\mathbf{z}^{(2)}\right) & \dots & \Phi_{N_\mathrm{p}-1}\left(\mathbf{z}^{(2)}\right) \\ \vdots & \vdots & \ddots & \vdots \\ \Phi_0\left(\mathbf{z}^{(N_\mathrm{s})}\right) & \Phi_1\left(\mathbf{z}^{(N_\mathrm{s})}\right) & \dots & \Phi_{N_\mathrm{p}-1}\left(\mathbf{z}^{(N_\mathrm{s})}\right) \end{bmatrix}}_{\mathbf{M}} \underbrace{\begin{bmatrix} c_0 \\ c_1 \\ \vdots \\ c_{N_\mathrm{p}-1} \end{bmatrix}}_{\mathbf{c}} = \underbrace{\begin{bmatrix} f\left(\mathbf{z}^{(1)}\right) \\ f\left(\mathbf{z}^{(2)}\right) \\ \vdots \\ f\left(\mathbf{z}^{N_\mathrm{s}}\right) \end{bmatrix}}_{\mathbf{y}}. \tag{31}$$

The number of samples N_s should be equal to or greater than the number of unknown expansion coefficients N_p. It is recommended to use at least $N_\mathrm{s} = 2N_\mathrm{p}$ to obtain a good least squares minimization. In that case, the system (31) is overdetermined, and the best approximation is given by

$$\mathbf{c} = (\mathbf{M}^\mathrm{T}\mathbf{M})^{-1}\mathbf{M}^\mathrm{T}\mathbf{y}. \tag{32}$$

The samples may be obtained using any sampling method that covers the entire input domain. As a result, the number of samples required for the regression approach is generally less than the number of samples required for the projection approach, especially when $D \gg 1$ [14].

6.3. Uncertainty quantification

6.3.1. Statistical moments. The uncertainty measures can directly be obtained using the PC expansion by replacing f by f_PC from (24) in the definition of the statistical moments and making use of the orthogonality property (27) and the zero-mean property (26).

The expected value is simply its first expansion coefficient:

$$\begin{aligned} \mathbb{E}[Y] \approx \mathbb{E}_\mathrm{PC}[Y] &= \int_{\Omega_\mathbf{Z}} \sum_{e=0}^{N_\mathrm{p}-1} c_e \Phi_e(\mathbf{z}) \rho_\mathbf{Z}(\mathbf{z})\, \mathrm{d}\mathbf{z} \\ &= c_0. \end{aligned} \tag{33}$$

Similarly, the variance is merely a sum of squared expansion coefficients multiplied by known factors:

$$\begin{aligned} \mathbb{V}[Y] \approx \mathbb{V}_\mathrm{PC}[Y] &= \mathbb{E}\left[(f_\mathrm{PC}(\mathbf{Z}) - \mathbb{E}_\mathrm{PC}[Y])^2\right] = \int_{\Omega_\mathbf{Z}} (f_\mathrm{PC}(\mathbf{z}) - c_0)^2 \rho_\mathbf{Z}(\mathbf{z})\, \mathrm{d}\mathbf{z} \\ &= \int_{\Omega_\mathbf{Z}} \left(\sum_{e=0}^{N_\mathrm{p}-1} c_e \Phi_e(\mathbf{z}) \right)^2 \rho_\mathbf{Z}(\mathbf{z})\, \mathrm{d}\mathbf{z} - c_0^2 = \sum_{e=0}^{N_\mathrm{p}-1} c_e^2 \int_{\Omega_\mathbf{Z}} \Phi_e^2(\mathbf{z}) \rho_\mathbf{Z}(\mathbf{z})\, \mathrm{d}\mathbf{z} - c_0^2 \\ &= \sum_{e=0}^{N_\mathrm{p}-1} c_e^2 H_e - c_0^2 = \sum_{e=1}^{N_\mathrm{p}-1} c_e^2 H_e \end{aligned} \tag{34}$$

6.3.2. Percentiles and prediction intervals. Percentiles and prediction intervals for Y cannot be derived directly from its PC expansion. However, it is possible to obtain percentiles and intervals by applying the MC method and using f_PC instead of f to evaluate the samples. The procedure is then the same as explained in Section 5.

DOI: 10.1002/cnm

6.4. Sensitivity analysis

6.4.1. Variance-based sensitivity indices. The PC expansion can also directly be used to obtain the main and total sensitivity indices from simple algebraic expressions given in the succeeding paragraphs. By exploitation of the properties of the polynomials in the chaos expansion, we approximate the total variance in the output Y by

$$\mathbb{V}[Y] \approx \mathbb{V}_{\mathrm{PC}}[Y] = \sum_{\boldsymbol{\alpha}\in\mathcal{A}} \mathbb{V}\left[c_{\boldsymbol{\alpha}}\Phi_{\boldsymbol{\alpha}}(\mathbf{Z})\right] = \sum_{\boldsymbol{\alpha}\in\mathcal{A}} c_{\boldsymbol{\alpha}}^2 H_{\boldsymbol{\alpha}}. \tag{35}$$

Using Sobol's variance decomposition, it has been shown that the main index can be obtained from the expansion coefficients $c_{\boldsymbol{\alpha}}$ and evaluations of the analytical expressions of $H_{\boldsymbol{\alpha}}$ [21, 22]. By introducing the set $\mathcal{A}_i$

$$\mathcal{A}_i = \{\boldsymbol{\alpha} \mid \alpha_i > 0 \wedge \alpha_j = 0 \quad \forall\, j \neq i\}, \tag{36}$$

the main sensitivity index can be approximated by [14, 75]

$$S_i \approx \frac{1}{\mathbb{V}_{\mathrm{PC}}[Y]} \sum_{\boldsymbol{\alpha}\in\mathcal{A}_i} \mathbb{V}\left[c_{\boldsymbol{\alpha}}\Phi_{\boldsymbol{\alpha}}\right]. \tag{37}$$

For the total sensitivity index, we introduce the set $\mathcal{A}_{\mathrm{T},i}$

$$\mathcal{A}_{\mathrm{T},i} = \{\boldsymbol{\alpha} \mid \alpha_i > 0\}. \tag{38}$$

The total sensitivity index can be approximated by [14, 75]

$$S_{\mathrm{T},i} \approx \frac{1}{\mathbb{V}_{\mathrm{PC}}[Y]} \sum_{\boldsymbol{\alpha}\in\mathcal{A}_{\mathrm{T},i}} \mathbb{V}\left[c_{\boldsymbol{\alpha}}\Phi_{\boldsymbol{\alpha}}\right]. \tag{39}$$

Note that $\mathcal{A}_{\mathrm{T},i}$ includes all basis functions in which input Z_i is included.

7. PROCEDURE AND EXAMPLES

To facilitate the use of the MC and PC methods for UQ and SA, we will present a simple, generic procedure. The procedure will be demonstrated for two typical examples of cardiovascular models. The first model is designed to estimate fractional flow reserve, which is a measure for stenosis severity. The second model can be used to estimate total arterial compliance of an individual.

We first outline the steps involved in performing UQ and SA on any given model, followed by the presentation of the specific UQ and SA methods and settings that will be applied for the two examples. Finally, we present the results of applying these methods to the two examples.

7.1. Procedure

The non-intrusive methods typically follow the following six steps:

Step 1 Identification of the output(s) of interest Y
Step 2 Identification and assessment of the distribution of the uncertain inputs $\mathbf{Z}$
Step 3 Sampling of the input space to acquire samples $\left\{\mathbf{z}^{(s)}\right\}_{s=1}^{N_{\mathrm{s}}}$
Step 4 Evaluation of the deterministic model to obtain $\left\{\boldsymbol{y}^{(s)}\right\}_{s=1}^{N_{\mathrm{s}}}$
Step 5 Calculation of UQ and SA measures
Step 6 Assessment of convergence of UQ and SA measures

7.2. Configuration of Monte Carlo and Polynomial Chaos methods

The procedure will be applied using both MC and PC to obtain measures for UQ and SA.

DOI: 10.1002/cnm

7.2.1. Monte Carlo. Saltelli's procedure is used here. Two independent sampling matrices **A** and **B** (16) containing $N = 5 \cdot 10^3$ latin hypercube samples are created. After evaluation of the model for the samples in **A** and **B**, uncertainty is quantified by estimating the expected value and variance using (13) and (14), respectively. Additionally, a 95% prediction interval is obtained using the percentiles. For SA, the matrices $\mathbf{C}_i$ are generated from **A** and **B** for an additional $5 \cdot 10^3 D$ input samples (in total, $N_\mathrm{s} = 5 \cdot 10^3(D+2)$). After evaluation of the model for the new input samples, the main and total sensitivity indices are calculated using (18) and (21), respectively.

7.2.2. Polynomial chaos. The PC expansion is truncated to a maximal order of $p = 4$ resulting in a total of $N_\mathrm{p} = \binom{D+p}{D}$ polynomial basis functions with unknown coefficients. The expansion coefficients will be estimated using least-squares regression (32). To obtain good estimates, we use $N_\mathrm{s} = 2N_\mathrm{p}$, which are generated using the Sobol sequence. Uncertainty is quantified by the expected value and the variance, which are calculated using (33) and (34), respectively. A 95% prediction interval is created from output realizations obtained from evaluation of the PC expansion for $100N_s$ new input samples. For SA, the main and total sensitivity indices are calculated using (37) and (39), respectively.

7.2.3. Assessment of convergence. For convergence, we consider the variance for UQ and the total sensitivity indices for SA. We assume accurate estimates are obtained with MC at $N_\mathrm{s} = 5 \cdot 10^3(D+2)$ samples and define convergence as the minimum number of samples required to keep the relative error of the variance below 5% and the absolute error of the sensitivity indices below 3%.

For MC, convergence is governed simply the number of samples N_s. We compared the estimates of $\mathbb{V}_\mathrm{MC}$ and $S_{\mathrm{T},i}$ obtained with a logarithmically spaced number of samples between $N_\mathrm{s} = 10(D+2)$ and $N_\mathrm{s} = 5 \cdot 10^3(D+2)$ to assess the convergence of the obtained measures. For PC, the convergence is governed by the number of samples N_s and the maximal polynomial order p of the expansion. We compared the estimates for $\mathbb{V}_\mathrm{PC}$ and $S_{\mathrm{T},i}$ obtained with different polynomial expansions with orders between $p = 1$ and $p = 4$ and with sample sizes between $N_\mathrm{s} = 2N_\mathrm{p}$ to $N_\mathrm{s} = i_\mathrm{max}N_\mathrm{p}$ (where $N_\mathrm{p} = \binom{D+p}{p}$ the number of expansion coefficients and $i_\mathrm{max} = \text{lower}\left\lfloor \frac{N_\mathrm{s,max}}{N_\mathrm{p}} \right\rfloor$ the number of samples per expansion coefficient with $N_\mathrm{s,max} = 2\binom{D+4}{4}$). We assess whether there is convergence for each combination of p and $i (= [2, i_\mathrm{max}])$. For more rigorous convergence testing approaches, it is possible to use leave-one-out cross validation and parameterized bootstrapping. See, for example, Hastie [76] for more details.

7.3. Fractional flow reserve

7.3.1. Background. Fractional flow reserve is a clinical measure that is clinically useful to assess the severity of a coronary artery stenosis [77, 78]. The FFR (c_FFR) is the ratio between the flow through the stenosed vessel and the flow through that vessel in the absence of that stenosis under hyperemic conditions. The current method for assessing FFR requires invasive measurements of the pressures proximal (p_p) and distal p_d to the coronary stenosis. To avoid unnecessary catheterization of patients, researchers have attempted to assess c_FFR using computational methods and non-invasive imaging modalities. The pressures proximal and distal to the stenosis are assessed using 3-D computational fluid dynamics (CFD) simulations on a patient-specific coronary artery domains [79, 80]. However, as these computations are computationally expensive, less computationally expensive, lumped-parameter models are also being investigated. One such lumped parameter model has been developed by Huo *et al.* [81]. Huo's model predicts the pressure drop over the stenosis based on six geometrical and four hemodynamic parameters and agrees well with experimental measurements. The geometrical parameters may be assessed from angiography images, whereas the hemodynamic parameters must be estimated.

7.3.2. Procedure.

Step 1: Although Huo's model predicts pressure drop, the output of interest considered in this example is the FFR, which can be easily derived from the predicted pressure drop and

DOI: 10.1002/cnm

Table II. Input and their uncertainties for the fractional flow reserve model in a hypothetical patient-specific case.

Nr.	Symbol	Description	Value	Unit	Uncertainty (%)
1	l_p	Proximal length	10	mm	5
2	l_s	Stenosis length	10	mm	5
3	l_d	Distal length	5	mm	5
4	r_p	Proximal radius	1.90	mm	5
5	r_p	Stenosis radius	0.55	mm	5
6	r_p	Distal radius	1.70	mm	5
7	q_h	Hyperemic blood flow	1	$\mathrm{ml{\cdot}min^{-1}}$	10
8	p_a	Arterial pressure	12	kPa	10
9	v	Blood viscosity	3.5	mPa·s	2
10	d	Blood density	1040	$\mathrm{kg{\cdot}m^{-3}}$	2

the proximal pressure input:

$$c_\mathrm{FFR} = f_\mathrm{FFR}(\mathbf{z}) = f_\mathrm{FFR}(l_\mathrm{p}, l_\mathrm{s}, l_\mathrm{d}, r_\mathrm{p}, r_\mathrm{s}, r_\mathrm{d}, p_\mathrm{a}, q_\mathrm{h}, v, d), \tag{40}$$

where c_FFR is the FFR value and the inputs $l_\mathrm{p}, l_\mathrm{s}, l_\mathrm{d}$ are proximal, stenosis, and distal lengths; $r_\mathrm{p}, l_\mathrm{s}, r_\mathrm{d}$, are the corresponding lumen radii; p_a is the arterial (proximal) pressure; q_h is the hyperemic flow; and v, d are the dynamic blood viscosity and density, respectively. A more detailed description of the model can be found in Appendix C.

Step 2: We consider a hypothetical case where inputs have been assessed for a specific patient. The geometrical inputs (lengths, radii) can be assessed from computed tomography (CT) data by segmenting the lumens with $\pm 5\%$ uncertainty. The arterial pressure p_a is set to the mean brachial artery pressure, which can be measured by sphygmomanometry. Because proximal coronary pressure likely deviates from brachial pressure, the uncertainty of p_a is set to $\pm 10\%$. The hyperemic flow q_h must be approximated, for example, by first estimating the total coronary flow based on myocardial volume from CT and then estimating the flow through the stenosed artery by using Murray's law [79]. We assume that the uncertainty in q_h is therefore $\pm 10\%$. The uncertainties in the density and viscosity of blood are based on population statistics, leading to $\pm 2\%$ uncertainty for both variables. The resulting input ranges (Table II) correspond to a 100% confidence interval for the arbitrarily chosen physiological case.

Step 3: The FFR model has $D = 10$ uncertain inputs so the total number of samples used for MC is $N_\mathrm{s} = 60000$; for PC, $N_\mathrm{s} = 2002$, and Legendre polynomials are used as the basis set because the random inputs are uniformly distributed.

Step 4: The FFR values c_FFR are obtained for each input sample $\mathbf{z}$ using f_FFR (40).

Step 5: Measures for UQ and SA are calculated using MC and PC as described.

Step 6: Monte Carlo estimates required at least $N_\mathrm{s} = 1831(D+2) = 21972$ samples for convergence of the variance and at least $N_\mathrm{s} = 1920(D+2) = 23040$ samples for convergence of the total sensitivity indices. PC estimates required at least $N_\mathrm{s} = [22, 132, 572, 2002]$ for respectively $p = [1, 2, 3, 4]$ to achieve convergence of the variance estimate and the total sensitivity indices.

7.3.3. Results. The PC method can yield the same results as the MC method, but at a significantly lower computational cost. Figure 3 shows the distribution of the FFR as calculated by MC (top) and PC (bottom). The distribution, which is similar for both methods, is asymmetric with a longer tail towards the lower FFR values. As a result, the mean value is lower than the median. The mean, the standard deviation, and the 95% prediction interval are given in Table III.

Figure 4 shows the main and total sensitivity indices obtained using both MC and PC methods. Of all considered inputs, only the stenotic radius r_s ($S_\mathrm{T} \approx 0.56$), the hyperemic flow q_h ($S_\mathrm{T} \approx 0.3$), and the arterial pressure p ($S_\mathrm{T} \approx 0.14$) significantly contribute to the variance in the FFR. There do not seem to be any interactions between inputs present because the main indices are approximately the same as the total indices ($S_i \approx S_{\mathrm{T},i}$).

DOI: 10.1002/cnm

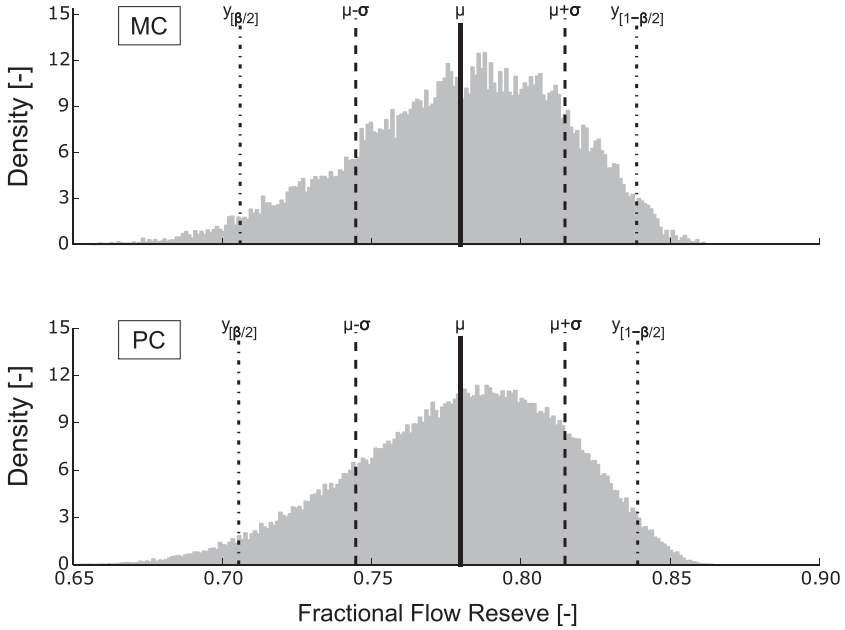

Figure 3. The numerically evaluated distributions of the fractional flow reserve model values obtained with Monte Carlo (MC) using $N_s = 60000$ samples (top) and with a polynomial chaos (PC) of maximal order $p = 4$ using $N_s = 2002$ samples (bottom). In vertical bars, the mean (thick line), mean $\pm$ standard deviation (dashed lines), and the bounds of the 95% prediction interval (dot-dashed lines) are shown.

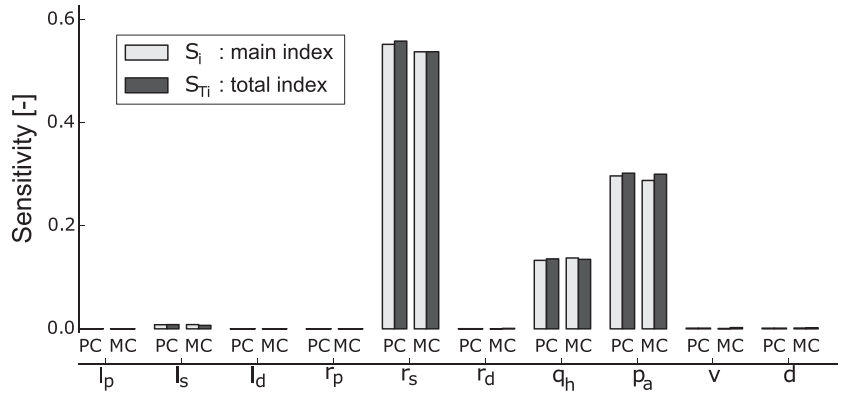

Figure 4. The Sobol indices for the fractional flow reserve model, S_i gray and $S_{T,i}$ black, are shown as bars. They are grouped by the uncertain input shown on the horizontal axis. The estimates from the polynomial chaos (PC) method are shown by the left two bars of each group, left being S_i and right being $S_{T,i}$. The two subsequent bars show Monter Carlo (MC) estimates of S_i and $S_{T,i}$ respectively.

Table III. Results of the UQ of the FFR model for MC and PC with uncertainties presented in Table II as well as the reduced uncertainty estimated using PC and input uncertainty corresponding to hypothetical improved measurement methods (Imp).

Method	Mean [-]	Standard deviation [-]	95% Prediction interval [-]
MC	0.78	0.035	[0.71, 0.84]
PC	0.78	0.035	[0.71, 0.84]
Imp	0.78	0.018	[0.73 0.74]

UQ, uncertainty quantification; FFR, fractional flow reserve; MC, Monte Carlo; PC, polynomial chaos.

DOI: 10.1002/cnm

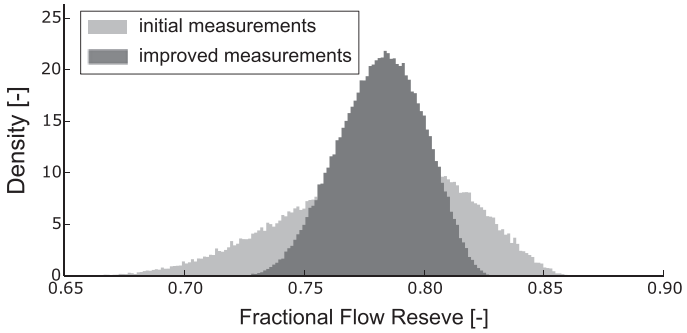

Figure 5. Comparison of estimated density for the fractional flow reserve model using the uncertainties presented in Table II (light gray) to by half reduced uncertainties in the stenotic radius, the hyperemic flow, and the proximal pressure (dark gray).

7.3.4. Discussion. Typically, in clinical application of FFR, the cases with FFR values below 0.8 are considered eligible for coronary intervention. The significant uncertainty in the predicted FFR, c_{FFR}, may lead to the wrong decisions about coronary intervention when using it in a clinical setting. For clinical application, it is therefore desirable to reduce the uncertainty in c_{FFR}. The sensitivity analysis clearly shows that the prediction of FFR can be improved most efficiently by reducing the inaccuracies in the measurements of the stenotic radius, the hyperemic flow, and the proximal pressure. To illustrate this fact, we have conducted an additional uncertainty quantification in the hypothetical case that the uncertainty in the stenotic radius, the hyperemic flow, and the proximal pressure are reduced by half. Figure 5 shows the distribution of the FFR for scenario where the input uncertainties are reduced.

7.4. Total arterial compliance

7.4.1. Background. Many studies have identified changes in C_{T} as a statistically significant factor associated with general health as well as several particular diseases (e.g., diabetes, hypertension, and etc.) [82–84]. The pulse pressure (PP) method was introduced by Stergiopulos *et al.* to estimate C_{T} using easily performed (i.e., non-invasive) clinical measurements of systolic and diastolic pressures [85, 86]. The PP method estimates C_{T} by minimization of the difference between the measured pressures and the pressures simulated using a Windkessel model consisting of a resistance R and the compliance C_{T} that is driven by cardiac outflow $q(t)$. In this example, $q(t)$ is a generic periodic function that matches the measured heart rate h and the mean cardiac output, which is estimated from measurements of the heart rate h and stroke volume V_{s}. The resistance in the Windkessel model estimated by Ohm's law: $R = p_{\mathrm{m}}/q_{\mathrm{m}}$, with p_{m} the mean pressure estimated by $p_{\mathrm{m}} = p_{\mathrm{d}}+(p_{\mathrm{s}}-p_{\mathrm{d}})/3$ and the q_{m} the mean flow (cardiac output) estimated by $q_{\mathrm{m}} = hV_{\mathrm{s}}$.

7.4.2. Procedure.

Step 1: The output of interest is the total compliance C_{T}, which is estimated using the PP method that is represented in black-box form as

$$C_{\mathrm{T}} = f_{\mathrm{PP}}(\mathbf{z}) = f_{\mathrm{PP}}(p_{\mathrm{s}}, p_{\mathrm{d}}, V_{\mathrm{s}}, h), \tag{41}$$

where p_{s} is the systolic pressure, p_{d} is the diastolic pressure, V_{s} is the stroke volume, and h is the heart rate. A more detailed description of the method can be found in Appendix C.

Step 2: The inputs of f_{PP} can all be assessed non-invasively by methods that are uncertain because of the accuracy of the procedure itself (e.g., indirect measurements, low resolution, and noise), as well as errors and subjective observations by the operator. Each input is modeled as a normally distributed random variable with a mean value and a standard deviation. This assumes that the measurement methods used, although imprecise, yield accurate input values (i.e., they are unbiased).

DOI: 10.1002/cnm

To assess systolic and diastolic blood pressures (p_s, p_d), mercury sphygmomanometers are still considered the gold standard of all non-invasive devices [87]. The accuracy of the method is dependent on the posture of the patient, cuff-size, and skill of the operator [12]. We set the standard deviation for systolic and diastolic pressures to those found in [88, Table II].

The stroke volume V_s of patients may be measured through ultrasound or MRI methods. One study on the accuracy of these methods shows variations of up to 20–30 ml discrepancy between the methods [89], thus we set the standard deviation to a third of this such that samples from a normal distribution have a 99% probability of lying with 24 ml of the mean.

The heart rate h is commonly measured by counting the pulse for 15 s and multiplying the result by 4. Miscounting by a single beat therefore results in a heart rate that differs from the actual value by 4 beats per minute. We account for this by setting the standard deviation of h to 4. The distributions of the uncertain input are summarized in Table IV.

Step 3: The model has $D = 4$ uncertain inputs so the total number of samples used for MC is $N_s = 30000$; for PC, $N_s = 280$, and Hermite polynomials are used as the basis set because the random inputs are normally distributed.

Step 4: The total compliance C_T is obtained for each input sample $\mathbf{z}$ using f_{PP}.

Step 5: Measures for UQ and SA are calculated using MC and PC as described.

Step 6: Monte Carlo estimates required at least $N_s = 1950(D+2) = 13266$ samples for convergence of the variance and at least $N_s = 1616(D+2) = 9696$ samples for convergence of the total sensitivity indices. PC estimates required at least $N_s = [10, 30, 70, 140]$ for respectively $p = [1, 2, 3, 4]$ to achieve convergence of the variance estimate and the total sensitivity indices.

7.4.3. Results and discussion. Monte Carlo and PC estimates of the uncertainty and sensitivity measures were found to correspond well. Figure 6 shows the density of estimates of the total compliance as obtained with MC (top) and PC (bottom). We observe C_T has a significant amount of variance and an asymmetric distribution. The estimates for the expected value, the standard deviation, and the 95% prediction interval can be found in Table V. The measures of uncertainty show that the PP method estimates C_T with a large amount of uncertainty, as Liu *et al.* [90] suggest a change in C_T from 1.47 to 1.07 from healthy individuals to hypertensive.

Table IV. Mean and standard deviations of the random normal inputs Z_i for the pulse pressure method to estimate total arterial compliance C_T.

Nr.	Symbol	Description	Unit	Mean (μ)	Standard deviation (σ)
1	h	Heart rate	bpm	65	4
2	V_s	Stroke volume	ml	75	8
3	p_s	Systolic pressure	mmHg	115	3.3
4	p_d	Diastolic pressure	mmHg	75	5.5

Table V. Results of the UQ of the total compliance C_T [ml/mmHg] for MC and PC with uncertainties presented in Table IV as well as the reduced uncertainty estimated using PC and input uncertainty corresponding to hypothetical improved measurement methods (Imp).

Method	Mean [ml/mmHg]	Standard deviation [ml/mmHg]	95% Prediction interval [ml/mmHg]
MC	1.46	0.31	[0.99, 2.16]
PC	1.46	0.30	[0.98, 2.19]
Imp	1.42	0.09	[1.26, 1.62]

UQ, uncertainty quantification; MC, Monte Carlo; PC, polynomial chaos.

DOI: 10.1002/cnm

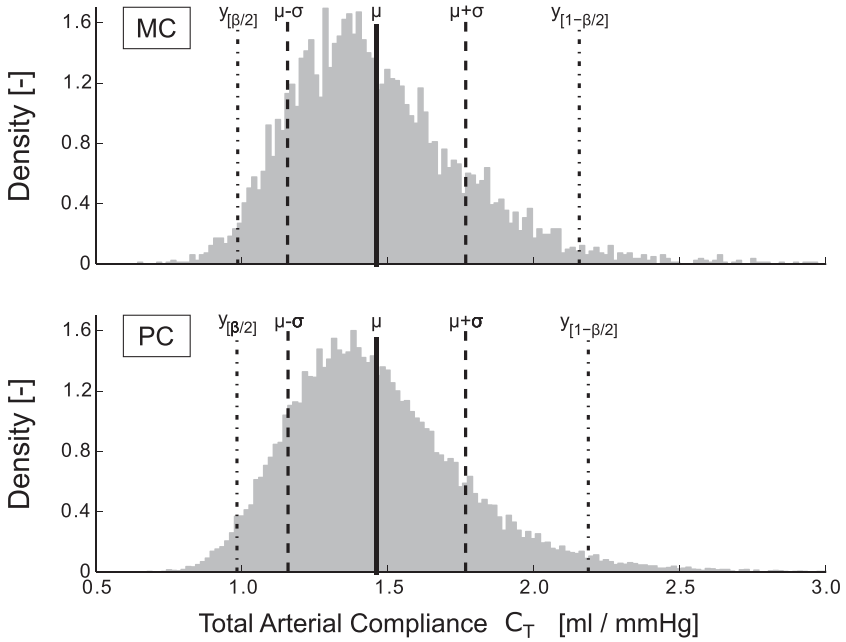

Figure 6. The resulting densities, evaluated numerically, for C_{T}, Monte Carlo (MC) with $N_{\mathrm{s}} = 30\,000$ on top, and polynomial chaos (PC) order 4 under. The center vertical line denotes the estimated value of $\mu(C_{\mathrm{T}})$ and the dashed lines to either side denote $\mu(C_{\mathrm{T}}) \pm \sigma(C_{\mathrm{T}})$. In vertical bars, the mean (thick line), mean $\pm$ standard deviation (dashed lines), and the bounds of the 95% prediction interval (dot-dashed lines) are shown.

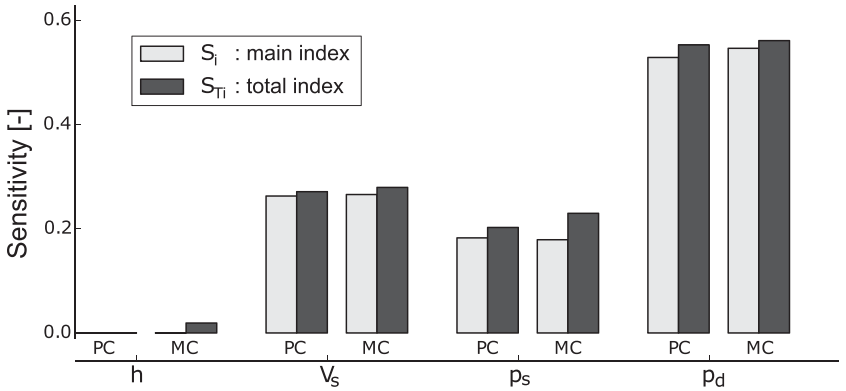

Figure 7. The Sobol indices for the pulse pressure method of estimating C_{T}, S_i gray, and $S_{\mathrm{T},i}$ black, are shown as bars. They are grouped by the uncertain input shown on the horizontal axis. The estimates from the polynomial chaos (PC) method are shown by the left two bars of each group, left being S_i and right being $S_{\mathrm{T},i}$. The two subsequent bars show Monte Carlo (MC) estimates of S_i and $S_{\mathrm{T},i}$ respectively.

Figure 7 shows a comparison of the main and total sensitivity indices, where the results of MC and PC correspond well. The uncertainty in the total compliance is largely because of uncertainties in the diastolic pressure ($S_4 \approx 0.53$), the stroke volume ($S_2 \approx 0.26$), and the systolic pressure ($S_3 \approx 0.18$). Moreover, there is some interaction between the diastolic pressure, the systolic pressure, and the stroke volume. The contribution of the heart rate is negligible.

The results suggest that improving measurements of V_{s}, p_s, and p_d may reduce the uncertainty in estimates of C_{T}, thus we considered a hypothetical case where V_{s} is measured using MRI, which has a typical error of 8 ml, and an improved pressure measurement which reduced the standard deviation by a factor of three. The resulting estimate for the density of C_{T} is shown in Figure 8, and the resulting estimates of the mean, standard deviation, and 95% prediction interval are included in Table V.

DOI: 10.1002/cnm

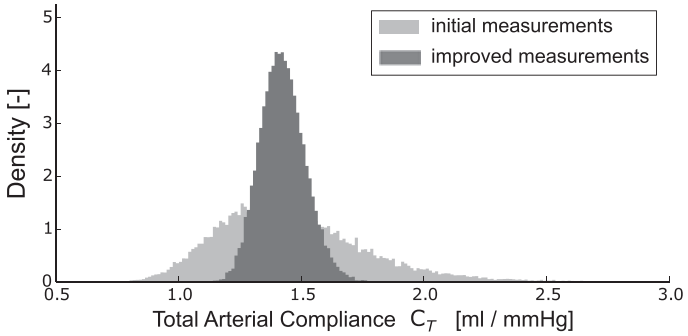

Figure 8. Comparison of estimated density of the pulse pressure estimate of C_T using the uncertainties reported in Table IV (light gray) to that from reducing the uncertainty of V_s, p_s, and p_d to standard deviations of 2.6 ml, 1.1 mmHg, and 1.8 mmHg, respectively (dark gray).

8. DISCUSSION

In this article, we aimed to give a brief and easily understandable guide for UQ and SA using methods that are readily available for application in biomedical engineering. We have explained two non-intrusive methods that do not require changes to the model code: the MC method and the PC method. In addition, we have provided a procedure containing six steps for performing UQ and SA. Both the MC and PC methods were applied successfully by following the six-step procedure for two clinical relevant models in which UQ and SA can give valuable insights, which will be elaborated on here. Both methods were found to yield the same conclusions with respect to UQ and SA, albeit at different computational costs. Further, we demonstrated that sensitivity analysis is useful in identifying how to reduce output uncertainty by improving measurement of sensitive inputs. In the following discussion, we address some questions regarding the applicability of both methods, as well as some limitations of our overview.

8.1. Example and applications

8.1.1. Procedure application. For both examples, MC and PC estimates of the uncertainty and sensitivity measures were found to correspond very well. The two models are quite contrasting in complexity, but both demonstrate the importance of considering uncertainty in model output, as well as the value of SA in understanding which inputs are most significant on output uncertainty. The results for example 1 (FFR) show that the Huo model can produce estimates with a large uncertainty in the FFR value (c_FFR) under current assumptions of uncertainties in the inputs. If this hypothetical case was considered by clinicians, the uncertainty in the FFR may be too high for the model to be used as an estimate for the true FFR value. The uncertainty measures indicate a large interval of likely values on both sides of $c_\mathrm{FFR} = 0.8$, the typical cut-off value to decide on coronary intervention. The SA also reveals that the uncertain inputs r_s (stenotic radius), p_a (pressure proximal to stenosis), and q_h (the hyperemic flow) contribute the most to the variance (uncertainty) in c_FFR. Consequently, to reduce the uncertainty in c_FFR, they need to be measured more precisely. The remaining parameters can each be fixed within its uncertainty interval, as the uncertainty in the measurement does significantly propagate to uncertainty in the FFR (input fixing). By reducing the uncertainty in the three most relevant parameters, we have shown to be able to reduce the uncertainty in c_FFR.

The results for example 2 (C_T-estimation) show that the PP method estimates C_T with an amount of uncertainty that is too large compared with the differences observed between healthy and hypertensive individuals [90]. Furthermore, the results show that uncertainty in the total compliance is largely because of uncertainties in the diastolic pressure, systolic pressure, and the stroke volume. Although the first two of these are routinely measured in the clinic, the current methodologies are not sufficiently accurate to allow effective estimation of C_T. This example further argues the need for UQ and SA because even simple model applications such as the PP estimation method may turn out to be highly sensitive to measurement uncertainty. As with the first example, we considered

DOI: 10.1002/cnm

the uncertainty of the estimated C_T using hypothetically more accurate measurement modalities for stroke volume and blood pressure. Much better estimates of C_T were obtained after reducing the uncertainties in these inputs, although the prediction interval was still quite wide compared with the measured difference between healthy and unhealthy individuals. For the uncertainties considered, the results suggest that the pulse pressure method may not be sufficiently accurate to distinguish between healthy and diseased states.

The results from both examples emphasize the relevance of UQ and SA in clinical application as they show the difficulties in assessing even 'basic' parameters associated with common cardiovascular diseases (e.g., coronary stenosis and hypertension).

8.2. A comparison of Monte Carlo and polynomial chaos

As our examples (Section 7) point out, both MC method and the PC method perform well for UQ and SA. Naturally, the question arises of which method to use for your specific application. There are several differences between MC and PC to consider: the required pre-processing and post-processing, robustness, necessary assumptions, the obtained information, and the required number of samples. For clarity, we repeat that the PC must be used in conjunction with one of two possible approaches for obtaining the expansion coefficients: projection or regression.

Necessary assumptions. The MC does not require any assumptions. In PC, it is assumed that the stochastic output can be described using smooth polynomials of the stochastic input. Furthermore, PC method requires that the truncation of the PC expansion is chosen correctly to capture the effects of the uncertain inputs on the output. The simplest truncation scheme includes all polynomials up to a total polynomial degree p. The appropriate value for p is difficult to choose a priori. To capture possible interactions, the researcher must set $p > 1$. In our experience, $p = 4$ is generally sufficient to capture the outcomes of physical phenomena.

Pre-processing and post-processing. The MC method does not require additional pre-processing or post-processing steps. The PC requires additional pre-processing and post-processing steps: the polynomials in the expansion must be evaluated for all input samples (pre) and the expansion coefficients must be obtained using a projection or a regression approach (post).

Robustness. It is possible that the model under investigation is unable to yield an outcome for one or more input samples. The MC method is robust for missing outcome realizations as long as the remaining number of outcome realization is large enough. The robustness of the PC method depends on the approach used to obtain the expansion coefficients. For the projection approach, the expansion coefficients are obtained with a quadrature rule, which is not robust for missing output realizations. Also, its performance will suffer when the output behaves non-smoothly with respect to the inputs [14]. Alternatively, for the regression approach, the expansion coefficients are obtained by solving a least-squares problem, which is robust for missing output realizations as long as enough realizations remain.

Obtained information. For UQ, there is no difference between the MC and PC methods regarding the obtained information. (Note, however, that a second post-processing step needs to be conducted to calculate the percentiles using PCE; Section 6.3.2). For SA, the MC method yields only the main and total sensitivity indices when applying Saltelli's procedure, whereas the PC method also yields all higher-order sensitivity indices. (Note that it is possible to calculate all indices with MC method, but this is not computationally efficient). Moreover, the PC yields a functional relationship between model inputs and outputs (i.e., the PC expansion).

Required number of samples. The required number of samples (N_s) is dependent on the problem and the sampling scheme. It is therefore good practice to check for the convergence of the UQ and SA measures by increasing N_s. For both MC and PC, there are some rules of thumb:

In the case of UQ using the MC method, N_s is independent of D and $N_s = \mathcal{O}(10^4)$. For SA, the MC method requires $N_s = N(D + 2)$ samples, where $N = \mathcal{O}(10^3)$ [57]. In addition, it has been shown that for the same N_s, quasi-random sampling is more efficient than Latin hypercube and random sampling [91].

N_s for the PC methods depends on D and the approach used to obtain the expansion coefficients (Section 6). For the projection approach, N_s depends on the quadrature rule applied, for example, if tensor quadrature is applied, the required number of samples are $N_s = (p + 1)^D$. Alternatively, if

DOI: 10.1002/cnm

sparse grid quadrature is used, the required number of samples $N_s = \mathcal{O}\left((p+1)\log(p+1)^{D-1}\right)$ [71]. For the regression approach, a rule of thumb is $N_s \geq 2N_p$,where N_p is the number of unknown expansion coefficients $N_p = \binom{D+p}{p}$.

Summary. The MC method is more robust, it requires fewer assumptions, and it does not require additional pre-processing and post-processing steps. However, it does not yield higher-order sensitivity indices and requires much more samples than the PC method for low numbers of dimensions D (Figure 9). The PC method is a convenient and efficient alternative to the MC method. The required pre-processing and post-processing can be performed using readily available implementations, for example, from `chaospy` [51], the `GPC` package [92], and `Dakota` [52]. In addition, the assumption for the maximal polynomial order p can be checked by considering other values of p during post-processing and comparing the obtained results for UQ and SA. It is not recommended to use PC when the number of uncertain inputs is large (Figure 9). However, there are ways around this issue, which will be discussed in the next section.

8.3. Computationally expensive models

Models may have a high number of uncertain inputs (large dimension D) or a high computational cost of a single model evaluation (e.g., 3-D CFD). In such cases, the required number of samples N_s may become prohibitively high for performing UQ and/or SA for both the MC and the PC method. There are two general ways to overcome these problems: the number of uncertain inputs must be reduced or the required number of model evaluations must be reduced.

8.3.1. Reducing the number of uncertain inputs. The elementary effects method of Morris can be used to screen for uncertain inputs that have a non-significant effect on a model output at a relative low number of model evaluations [93, 94]. After screening, the identified non-influential uncertain inputs are no longer considered to be uncertain. They will be fixed within their uncertainty domain (in general the mean value). Only the remaining uncertain inputs are considered in subsequent MC or PC methods, which reduces the number of samples required for UQ and SA. Excellent results were obtained when the screening was combined with a PC method to perform SA of a pulse wave propagation model by Donders *et al.* [75].

8.3.2. Reducing the number of required model evaluations. In the case of models with very high computational costs (e.g., in 3-D CFD), advanced algorithms for the PC method that minimize the required number of model evaluations (i.e., number of samples N_s) may offer a solution. The number of required model evaluations depends on whether the regression or projection approach is used to determine the expansion coefficients c_e.

For the regression approach to avoid an underdetermined system, the number of model evaluations should be at least the same as the number of expansion coefficients: $N_s \geq N_p$. In practice, the number of evaluations is recommended to be an integer (≥ 2) multiple of the number of expan-

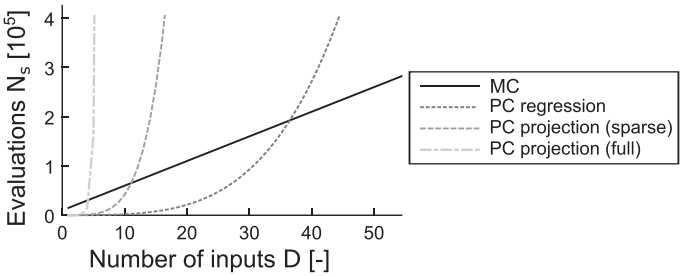

Figure 9. Number of samples for performing sensitivity analysis using different methods: Monte Carlo (MC) assuming $N_s = 5000\ D$ (solid black), polynomial chaos (PC) ($p = 4$) with regression assuming $N_s \geq 2N_p$ (dotted dark gray), PC with projection using sparse grid interpolation with level $l = p + 1$ (dashed gray), and PC with projection using the full tensor grid interpolation with $N_{1-D} = p + 1$ nodes in the $1 - D$ integration rule (dash-dotted light gray).

DOI: 10.1002/cnm

sion coefficients. Reducing the number of expansion coefficients consequently reduces the number of evaluations, that is, N_s. This can be performed by lowering the total polynomial order, which then introduces an additional truncation error. However, Blatman *et al.* have suggested alternative truncation schemes based on the assumption that in general, interaction effects contribute less than direct effects [95]. While maintaining the same total polynomial order, certain interaction effects are excluded to obtain a sparse polynomial chaos expansion. Blatman *et al.* have also introduced alternative algorithms that adaptively build up the PC expansion until some target accuracy is obtained [68, 95, 96].

For the projection approach, the number of model evaluations is determined by the quadrature rule applied to approximate the projection integral. Sparse grid quadratures are generally used even for relatively low numbers of uncertain inputs, where the most common Smolyak's algorithm creates an isotropic grid in all input dimensions. However, there may be some input directions in which a low quadrature order is sufficient for the accurate approximation of the projection integral. Hence, anisotropic sparse grids that have quadrature orders that correspond to the requirements in each input direction may improve the convergence. Adaptive dimension algorithms for sparse grids have been developed [97, 98]. Applications to UQ and SA are found in [99–101].

We remark that there are alternative approaches to reduce the number of polynomial bases of the PC expansion, which are independent of the applied method to calculate the PC expansion coefficients as the adaptive ANOVA decomposition [102] or Bayesian compressive sensing methods [103].

8.4. Limitations

8.4.1. Dependent uncertain inputs. We considered all uncertain inputs $\mathbf{Z}$ as independent random variables, which is not always true for all cardiovascular model inputs (e.g., arterial radius and arterial wall thickness are often considered dependent). However, the relationship of dependence is for most cases unknown. In case of dependent inputs, the sensitivity analysis based on the Sobol decomposition is no longer applicable because the sensitivities are no longer additive and thus difficult to interpret [104]. Recent works have addressed this problem and provided theory for performing variance-based SA with dependent inputs [105–107]. For the PC method, the state of the art approach is to transform the dependent random variables to independent random variables with, for example, a Nataf [108] or Rosenblatt transformation [109], or to construct a dependent orthogonal expansion directly [110]. To our knowledge, no effort was made to apply dependent random variables in UQ and SA with the methods presented in this article in cardiovascular applications.

8.4.2. Time or spatially varying uncertain inputs. The methods presented in this article may also be applied in the case of uncertain inputs, which are time-varying or spatially varying (i.e., random fields). A random field can be seen as the collection of a high or infinite number of random variables. Such random fields often exhibit temporal or spatial correlation that can be exploited. A common approach is to use dimension reduction techniques to make the number of dimensions (i.e., number of random variables of the field) more manageable. For high-dimensional and infinite-dimensional processes, respectively, one may employ either principal component analysis [39] or Karhunen–Loeve expansion [36].

8.4.3. Alternative methods. In this article, we mention only the standard MC technique and the more advanced PC method, because they have been used the most in biomedical engineering [5, 14, 25, 27, 32, 33, 75]. However, there are other non-intrusive methods that may be used to perform UQ and SA that have been used for biomedical engineering models. Therefore, we give a brief overview of these alternative methods and their applications.

We first note that the PC method is a special member from the class of metamodeling methods. Metamodeling methods are methods that attempt to represent the response of the model using computationally inexpensive functions (polynomials, splines, generalized linear models, and Gaussian processes). These metamodels (also called *surrogate models* or *response surfaces*) can then be substituted for the model in the MC method for obtaining measures for uncertainty and sensitiv-

DOI: 10.1002/cnm

ity. The PC expansion is a metamodel that can bypass the need to subject it to the MC method because measures for uncertainty and sensitivity can be derived from it analytically (Section 6). The Lagrangian interpolation (LI) method is another metamodeling method from which the measures for uncertainty [23, 101] and sensitivity [24] can be derived analytically. In LI, the metamodel is a Lagrangian interpolant that is constructed over the output space from output samples obtained for input samples that are members of a sparse grid [101]. LI has been applied in the context of UQ by Sankaran *et al.* [30] and variance-based SA by Chen *et al.* [31], although only first-order indices were obtained. The Gaussian process method models the model outcome as a Gaussian stochastic process [111, 112]. As a result, the metamodel itself is stochastic. However, the posterior means can be used as the surrogate outputs in the MC method to obtain information about uncertainty and sensitivity. It was recently used by Biehler *et al.* [34] for UQ in biomechanics and by Melis *et al.* [113] in fluid mechanics.

Uncertainty and sensitivity measures obtained with metamodeling approaches have two sources of errors: those resulting from inaccuracies of the metamodel and those resulting from the MC integration (with the exception of PC and LI). More accurate metamodels can be constructed by incorporating information from more model outcomes, but these may be computationally expensive to obtain. An active body of research is attempting to reduce the computational cost of obtaining an accurate uncertainty measures through metamodels by using multi-fidelity schemes. In multi-fidelity schemes, low-fidelity, computationally inexpensive models provide information that can be related to the high-fidelity, computationally expensive model outcomes with simple functions [114]. The low-fidelity model outcomes are obtained after performing simulations in which rougher approximations are used (e.g., coarser spatial discretization, larger time steps, and fewer linearization iterations). Multi-fidelity approaches combined specifically with PC or LI have been reported by Ng *et al.* [115] and with a Gaussian process by Biehler *et al.* [34]. So far, there is limited research on the use of multi-fidelity approaches for SA (see, e.g., [116]).

9. CONCLUSION

We explained two methods for UQ and SA, MC and PC, and have demonstrated how to apply them to two typical cases using a non-intrusive six-step procedure. The six-step procedure can conveniently be adapted to other mathematical models. Hence, the methods introduced here can be used for UQ and the personalization of patient-generic models to patient-specific conditions (SA) without requiring researchers to have a very detailed understanding of the underlying theory.

APPENDIX A: VARIANCE DECOMPOSITION

Sobol decomposed a function f into a series of summands of increasing dimensionality [42]:

$$\begin{aligned} f(\mathbf{Z}) = f_0 &+ \sum_{i_1=1}^{D} f_{i_1}(Z_{i_1}) + \sum_{i_1=1}^{D}\sum_{i_2>i_1}^{D} f_{i_1,i_2}(Z_{i_1}, Z_{i_2}) + \dots \\ &+ \sum_{i_1=1}^{D}\sum_{i_2>i_1}^{D}\cdots\sum_{i_s>i_{s-1}}^{D} f_{i_1,i_2,\dots,i_s}(Z_{i_1}, Z_{i_2}, \dots, Z_{i_s}) + \dots \\ &+ f_{1,2\dots D}(Z_1, \dots, Z_D), \end{aligned} \tag{A.1}$$

with increasing indices $1 \leqslant i_1 < i_2 < \dots < i_s \leqslant D$ and $f_0 = \mathbb{E}[Y]$ the expected value (5). Each summand $f_{i_1,i_2,\dots,i_s}$ has the following property:

$$\int_{\Omega_{i_1,i_2,\dots,i_s}} f_{i_1,i_2,\dots,i_s}(Z_{i_1}, Z_{i_2}\dots, Z_{i_s})\rho(z_{i_1})\rho(z_{i_2})\cdots\rho(z_{i_s})\,\mathrm{d}z_j = 0 \quad \forall j = i_1, i_2, \dots, i_s. \tag{A.2}$$

DOI: 10.1002/cnm

As a consequence of (A.2), all summands are orthogonal to each other, and the decomposition (A.1) is unique [42]. The variance of f is then

$$\begin{aligned}\mathbb{V}[Y] = &\sum_{i_1=1}^{D} V_{i_1} + \sum_{i_1=1}^{D}\sum_{i_2>i_1}^{D} V_{i_1,i_2} + \dots \\ &+ \sum_{i_1=1}^{D}\sum_{i_2>i_1}^{D}\cdots\sum_{i_s>i_{s-1}}^{D} V_{i_1,i_2,\dots,i_s} + \dots \\ &+ V_{1,2\dots D},\end{aligned} \tag{A.3}$$

where the variances $V_{i_1,i_2,\dots,i_s}$ are defined by

$$V_{i_1,i_2,\dots,i_s} = \int_{\Omega_{i_1,i_2,\dots,i_s}} f^2_{i_1,i_2,\dots,i_s}\left(Z_{i_1}, Z_{i_2}\dots, Z_{i_s}\right)\rho\left(z_{i_1}\right)\rho\left(z_{i_2}\right)\cdots\rho\left(z_{i_s}\right)\mathrm{d}z_{i_1}\,\mathrm{d}z_{i_2}\cdots\mathrm{d}z_{i_s}. \tag{A.4}$$

Normalization of (A.3) with the total variance $\mathbb{V}[Y]$ gives

$$\begin{aligned}1 = &\sum_{i_1=1}^{D} S_{i_1} + \sum_{i_1=1}^{D}\sum_{i_2>i_1}^{D} + S_{i_1,i_2} + \dots \\ &+ \sum_{i_1=1}^{D}\sum_{i_2>i_1}^{D}\cdots\sum_{i_s>i_{s-1}}^{D} S_{i_1,i_2,\dots,i_s} + \dots \\ &+ S_{1,2,\dots,D}.\end{aligned} \tag{A.5}$$

where the summands $S_{i_1,i_2,\dots,i_s}$ are the sensitivity indices.

APPENDIX B: POLYNOMIAL CHAOS

B.1. Wiener–Askey scheme

The Wiener–Askey scheme shows which polynomials are best to use corresponding to what distribution.

Table B.1. The Wiener–Askey scheme introduced by Xiu and Karniadakis [19].

Type	Distribution	Orthogonal polynomial Φ	Support
Continuous	Gaussian	Hermite	$(-\infty, \infty)$
	Gamma	Laguerre	$[0, \infty)$
	Beta	Jacobi	$[a, b]$
	Uniform	Legendre	$[a, b]$
Discrete	Poisson	Charlier	$\{0, 1, 2, \dots\}$
	Binomial	Krawtchouk	$\{0, 1, \dots, N\}$
	Negative binomial	Meixner	$\{0, 1, 2, \dots\}$
	Hypergeometric	Hahn	$\{0, 1, \dots, N\}$

B.2. Normalization factors

An exact expression for the normalization factors can be obtained by using the multi-indices $\boldsymbol{\alpha}$:

$$H_e \equiv H_{\boldsymbol{\alpha}} = \int_{\Omega_{\mathbf{Z}}} \Phi^2_{\boldsymbol{\alpha}}(\mathbf{z})\rho_{\mathbf{Z}}(\mathbf{z})\,\mathrm{d}\mathbf{z} = \mathbb{E}\left[\prod_{i=1}^{D}\phi^2_{\alpha_i}\right] = \prod_{i=1}^{D}\mathbb{E}\left[\phi^2_{\alpha_i}\right] = \prod_{i=1}^{D} h_i, \tag{B.1}$$

DOI: 10.1002/cnm

where h_i is the normalization factor of the univariate polynomial ϕ of order α_i. Analytical expressions for h_i can be found in literature [19, 69].

APPENDIX C: EXAMPLES

C.1. Fractional flow reserve

The model of Huo predicts a pressure drop Δp:

$$\Delta p = \frac{\rho q^2}{2} \left(\Delta p_{\mathrm{c}} + \Delta p_{\mathrm{d}} + \Delta p_{\mathrm{e}}\right), \tag{C.1}$$

where Δp_{c}, Δp_{d}, and Δp_{e} represent the convective, diffusive, and expansion pressures losses. The convective contribution is given by

$$\Delta p_{\mathrm{c}} = \frac{1}{A_d^2} - \frac{1}{A_p^2}. \tag{C.2}$$

The diffusive and expansion pressures losses depend on the length of the stenosis (l_{s}). A dimensionless radius r' is introduced for the entrance region of the stenosis:

$$l_{\mathrm{s}} = \frac{\rho q}{\pi \mu} \int_{r'}^{1} \frac{(1-r')(6+r')\left(1+4r'+9r'^2+4r'^3\right)}{5r'(3+2r')(3+2r'+r'^2)^2}\,\mathrm{d}r' \tag{C.3}$$

For $r\prime \geqslant 0.05$, the diffusive pressure drop is given by

$$\Delta p_{\mathrm{d}}^{r'\geqslant 0.05} = \frac{1}{A_s^2}\frac{96}{5} \int_{r'}^{1} \frac{1+4r'+9r'^2+4r'^3}{r'(3+2r')(3+2r'+r'^2)^2}\,\mathrm{d}r' + \int_{0}^{l_{\mathrm{v}}-l_{\mathrm{s}}} \frac{8\pi\mu}{A} q\,\mathrm{d}x, \tag{C.4}$$

where $l_{\mathrm{v}} = l_{\mathrm{p}} + l_{\mathrm{s}} + l_{\mathrm{d}}$. The expansion pressure drop is given by

$$\begin{aligned} \Delta p_{\mathrm{e}}^{r'<0.05} = &\left(\frac{1}{A_{\mathrm{s}}} - \frac{1}{A_{\mathrm{d}}}\right)^2 + \left(1-r'\right)^2 \\ &\times \left[2\left(\frac{1}{A_{\mathrm{s}}} - \frac{1}{A_{\mathrm{d}}}\right)\left(\frac{1}{A_{\mathrm{s}}} - \frac{1}{3A_{\mathrm{d}}}\right) - \left(\frac{1}{A_s} - \frac{1}{A_d}\right)^2\right], \end{aligned} \tag{C.5}$$

On the other hand, if $r' < 0.05$, the entrance length is first calculated as

$$l_{\mathrm{e}} = \frac{\rho q}{\pi \mu} \int_{0.05}^{1} \frac{(1-r')(6+r')(1+4r'+9r'^2+4r'^3)}{5r'(3+2r')(3+2r'+r'^2)^2}\,\mathrm{d}r'. \tag{C.6}$$

Then, the diffusive pressure drop is given by

$$\Delta p_{\mathrm{d}}^{r'<0.05} = \frac{1}{A_s^2}\frac{96}{5} \int_{0.05}^{1} \frac{1+4r'+9r'^2+4r'^3}{r'(3+2r')(3+2r'+r'^2)^2}\,\mathrm{d}r' + \int_{0}^{l_{\mathrm{v}}+l_{\mathrm{e}}} \frac{8\pi\mu}{A} q\,\mathrm{d}x \tag{C.7}$$

The expansion pressure drop is given by

$$\Delta p_{\mathrm{e}}^{r'<0.05} = 2\left(\frac{1}{A_s} - \frac{1}{A_d}\right)\left(\frac{1}{A_s} - \frac{1}{3A_d}\right). \tag{C.8}$$

DOI: 10.1002/cnm

C.2. Pulse pressure method

The pulse pressure method is based on using a 2-Element Windkessel model of the vascular network. Thus the total arterial compliance is represented as a compliance C_T in parallel with the total peripheral resistance R. The system is driven by a flow $Q(t)$ and gives rise to the following differential equation:

$$C_T \frac{dP}{dt} = Q(t) - \frac{P}{R} \tag{C.9}$$

which is fully specified by an initial condition $P(t_0) = P_0$. We denote the solution for a particular value of C_T as $P(t, C_T)$. The pulse pressure predicted by the Windkessel model for a given compliance C_T is defined as

$$PP_m(C_T) = \max(P(t, C_T)) - \min(P(t, C_T)) \tag{C.10}$$

where the max and min are over time. To estimate C_T, we define the error between $PP_m(C_T)$ and the measured pulse pressure $PP_d = P_s - P_d$ as

$$e(C_T) = \left(\frac{PP_m(C_T) - PP_d}{PP_d} \right)^2 \tag{C.11}$$

C_T is then estimated by solving the minimization problem as

$$C_T = \arg\min e(C_T). \tag{C.12}$$

This may be achieved by an appropriate numerical optimization method, that is, Brent's method, where the interval allowed for C_T is set to $(0.1, 5.0)$ ml/mmHg (a typical value for humans is near 1.5 ml/mmHg).

REFERENCES

1. Stergiopulos N, Young DF, Rogge TR. Computer simulation of arterial flow with applications to arterial and aortic stenoses. *Journal of Biomechanics* 1992; **25**(12):1477–88. (Available from: http://www.ncbi.nlm.nih.gov/pubmed/1491023).
2. Speelman L, Schurink GWH, Bosboom EMH, Buth J, Breeuwer M, van de Vosse FN, Jacobs MH. The mechanical role of thrombus on the growth rate of an abdominal aortic aneurysm. *Journal of Vascular Surgery* 2010; **51**(1): 19–26.
3. Bovendeerd PHM, Borsje P, Arts T, Van De Vosse FN. Dependence of intramyocardial pressure and coronary flow on ventricular loading and contractility: a model study. *Annals of Biomedical Engineering* 2006; **34**(12):1833–1845.
4. van der Horst A, Boogaard FL, van't Veer M, Rutten MCM, Pijls NHJ, Van De Vosse FN. Towards patient-specific modeling of coronary hemodynamics in healthy and diseased state. *Computational and Mathematical Methods in Medicine* 2013; **2013**:Article ID 393792, 15 pages.
5. Eck VG, Feinberg J, Langtangen HP, Hellevik LR. Stochastic sensitivity analysis for timing and amplitude of pressure waves in the arterial system. *International Journal for Numerical Methods in Biomedical Engineering* 2015; **31**(4).
6. Cox LGE, Loerakker S, Rutten MCM, de Mol BAJM, van de Vosse FN. A mathematical model to evaluate control strategies for mechanical circulatory support. *Artificial organs* 2009; **33**(8):593–603.
7. Schampaert S, Rutten MCM, van T Veer M, van Nunen LX, Tonino PAL, Pijls NHJ, van de Vosse FN. Modeling the interaction between the intra-aortic balloon pump and the cardiovascular system: the effect of timing. *American Society for Artificial Internal Organs Journal* 2013; **59**(1):30–6. (Available from: http://www.ncbi.nlm.nih.gov/pubmed/23263334).
8. van der Hout-van der Jagt MB, Oei SG, Bovendeerd PHM. A mathematical model for simulation of early decelerations in the cardiotocogram during labor. *Medical Engineering & Physics* 2012; **34**(5):579–589. (Available from: http://www.sciencedirect.com/science/article/pii/S1350453311002293).
9. Leguy CAD, Bosboom EMH, Gelderblom H, Hoeks APG, van de Vosse FN. Estimation of distributed arterial mechanical properties using a wave propagation model in a reverse way. *Medical Engineering & Physics* 2010; **32**(9):957–67. (Available from: http://www.ncbi.nlm.nih.gov/pubmed/20675178).
10. Wolters BJBM, Rutten MCM, Schurink GWH, Kose U, de Hart J, van de Vosse FN. A patient-specific computational model of fluid-structure interaction in abdominal aortic aneurysms. *Medical Engineering & Physics* 2005; **27**(10):871–83. (Available from: http://www.ncbi.nlm.nih.gov/pubmed/16157501).

DOI: 10.1002/cnm

11. Bode A, Caroli A, Huberts W, Planken N, Antiga L, Bosboom M, Remuzzi A, Tordoir J. Clinical study protocol for the ARCH project - computational modeling for improvement of outcome after vascular access creation. *The Journal of Vascular Access* 2011; **12**(4):369–76. (Available from: http://www.ncbi.nlm.nih.gov/pubmed/21667457).
12. Pickering TG, Hall JE, Appel LJ, Falkner BE, Graves J, Hill MN, Jones DW, Kurtz T, Sheps SG, Roccella EJ. Recommendations for blood pressure measurement in humans and experimental animals part 1: blood pressure measurement in humans: a statement for professionals from the subcommittee of professional and public education of the american heart association council on high blood pressure research. *Hypertension* 2005; **45**(1):142–161.
13. Mancia G, Ferrari A, Gregorini L, Parati G, Pomidossi G, Bertinieri G, Grassi G, di Rienzo M, Pedotti A, Zanchetti A. Blood pressure and heart rate variabilities in normotensive and hypertensive human beings. *Circ Res* 1983; **53**(1): 96–104.
14. Huberts W, Donders WP, Delhaas T, van de Vosse FN. Applicability of the polynomial chaos expansion method for personalization of a cardiovascular pulse wave propagation model. *International Journal for Numerical Methods in Biomedical Engineering* 2014; **30**(12):1679–1704.
15. Kleiber M, Hien TD. *The Stochastic Finite Element Method: Basic Perturbation Technique and Computer Implementation*. John Wiley & Sons, Ltd: Chicester, United Kingdom, 1992.
16. Kamínski M. *The Stochastic Perturbation Method for Computational Mechanics*. John Wiley & Sons, Ltd: Chichester, England, 2013.
17. Zhang D. *Stochastic Method for Flow in Porous Media*. Academic Press: San Diego, California, United States of America, 2001.
18. Ghanem R, Spanos PD. Polynomial chaos in stochastic finite elements. *Journal of Applied Mechanics* 1990; **57**(1):197–202.
19. Xiu D, Karniadakis GEM. The Wiener-Askey polynomial chaos for stochastic differential equations. *SIAM Journal on Scientific Computing* 2002; **24**(2):619–644.
20. Fishman GS. *Monte Carlo: Concepts Algorithms and Applications*. Springer-Verlag: New York, 1996.
21. Sudret B. Global sensitivity analysis using polynomial chaos expansions. *Reliability Engineering & System Safety* 2008; **93**(7):964–979.
22. Crestaux T, Le Maître O, Martinez JM. Polynomial chaos expansion for sensitivity analysis. *Reliability Engineering & System Safety* 2009; **94**(7):1161–1172.
23. Xiu D, Hesthaven JS. High-order collocation methods for differential equations with random inputs. *SIAM Journal on Scientific Computing* 2005; **27**(3):1118–1139.
24. Buzzard GT, Xiu D. Variance-based global sensitivity analysis via sparse-grid interpolation and cubature. *Communications in Computational Physics* 2011; **9**(3):542–567.
25. Xiu D, Sherwin SJ. Parametric uncertainty analysis of pulse wave propagation in a model of a human arterial network. *Journal of Computational Physics* 2007; **226**(2):1385–1407.
26. Osnes H, Sundnes J. Uncertainty analysis of ventricular mechanics using the probabilistic collocation method. *Biomedical Engineering, IEEE Transactions on* 2012; **59**(8):2171–2179.
27. Leguy CAD, Bosboom EMH, Belloum ASZ, Hoeks APG, van de Vosse FN. Global sensitivity analysis of a wave propagation model for arm arteries. *Medical Engineering & Physics* 2011; **33**(8):1008–1016. (Available from: http://www.sciencedirect.com/science/article/pii/S1350453311000841).
28. Grinberg L, Cheever E, Anor T, Madsen JR, Karniadakis GE. Modeling blood flow circulation in intracranial arterial networks: a comparative 3D/1D simulation study. *Annals of biomedical engineering* 2011; **39**(1):297–309. (Available from: http://www.ncbi.nlm.nih.gov/pubmed/20661645).
29. Pereira JMC, e Moura JPS, Ervilha AR, Pereira JCF. On the uncertainty quantification of blood flow viscosity models. *Chemical Engineering Science* 2013; **101**(0):253–265. (Available from: http://www.sciencedirect.com/science/article/pii/S0009250913003643).
30. Sankaran S, Marsden AL. A stochastic collocation method for uncertainty quantification and propagation in cardiovascular simulations. *Journal of biomechanical engineering* 2011; **133**(3):031001. (Available from: http://www.ncbi.nlm.nih.gov/pubmed/21303177).
31. Chen P, Quarteroni A, Rozza G. Simulation-based uncertainty quantification of human arterial network hemodynamics. *International Journal for Numerical Methods in Biomedical Engineering* 2013; **29**:698–721.
32. Huberts W, de Jonge C, van der Linden WPM, Inda Ma, Tordoir JHM, van de Vosse FN, Bosboom EMH. A sensitivity analysis of a personalized pulse wave propagation model for arteriovenous fistula surgery. Part A: identification of most influential model parameters. *Medical Engineering & Physics* 2013; **35**(6):810–26. (Available from: http://www.ncbi.nlm.nih.gov/pubmed/22964062).
33. Huberts W, de Jonge C, van der Linden WPM, Inda Ma, Passera K, Tordoir JHM, van de Vosse FN, Bosboom EMH. A sensitivity analysis of a personalized pulse wave propagation model for arteriovenous fistula surgery. Part B: identification of possible generic model parameters. *Medical Engineering & Physics* 2013; **35**(6):827–37. (Available from:http://www.ncbi.nlm.nih.gov/pubmed/22964064).
34. Biehler J, Gee MW, Wall Wa. Towards efficient uncertainty quantification in complex and large-scale biomechanical problems based on a Bayesian multi-fidelity scheme. *Biomechanics and Modeling in Mechanobiology* 2015; **14**(3):489–513. DOI: 10.1007/s10237-014-0618-0.
35. Gardiner CW. *Handbook of Stochastic Methods: For Physics, Chemistry and the Natural Sciences*. Springer-Verlag: Berlin, Germany, 1985.
36. Xiu D. *Numerical Methods for Stochastic Computations: A Spectral Method Approach*. Princeton University Press: Princeton, N.J, 2010.

37. O'Hagan A, Buck CE, Daneshkhah A, Eiser JR, Garthwaite PH, Jenkinson DJ, Oakley JE, Rakow T. *Uncertain Judgements: Eliciting Experts' Probabilities* (1 edition). John Wiley & Sons, Ltd.: Chichester, United Kingdom, 2006.
38. Gelman A, Carlin JB, Stern HS, Dunson DB, Vehtari A, Rubin DB. *Bayesian Data Analysis*, 3rd edn., CRC Press: Boca Raton, Florida, United States of America, 2014.
39. Jolliffe I. *Principal Component Analysis*. Springer-Verlag: New York, New York, United Sates of America, 2002. DOI:10.1002/9781118445112.stat06472/full.
40. Granger C, Newbold P. *Forecasting in Business and Economics*, 2nd edn., Emerald Group Publishing Limited: Bingley, United Kingdom, 1986.
41. Sobol IM. On sensitivity estimation for nonlinear mathematical models. *Matematischeskoe modelirovanie* 1990; **2**(1):112–118.
42. Sobol IM. Global sensitivity indices for nonlinear mathematical models and their Monte Carlo estimates. *Mathematics and Computers in Simulation* 2001; **55**:271–280.
43. Saltelli A, Ratto M, Anders T. *Global Sensitivity Analysis, The Primer*. John Wiley & Sons, Ltd: Chichester, United Kingdom, 2008.
44. Homma T, Saltelli A. Importance measures in global sensitivity analysis of nonlinear models. *Reliability Engineering and System Safety* 1996; **52**:1–17.
45. Caflisch RE. Monte Carlo and quasi-Monte Carlo methods. *Acta Numerica* 1998; **7**:1–49.
46. Mckay MD, Beckman RJ, Conover WJ. A comparison of three methods for selecting values of input variables in the analysis of output from a computer code. *Technometrics* 1979; **21**(2):239–245.
47. Morokoff WJ, Caflisch RE. Quasi-random sequences and their discrepancies. *SIAM Journal on Scientific Computing* 1994; **15**(6):1251–1279.
48. Niederreiter H. Low-discrepancy and low-dispersion sequences. *Journal of Number Theory* 1988; **30**:51–70.
49. James F. Monte Carlo theory and practice. *Reports on Progress in Physics* 1980; **43**(9):1145. (Available from: http://iopscience.iop.org/0034-4885/43/9/002).
50. Reuven Y, Rubinstein DPK. *Simulation and the Monte Carlo Method 2nd Edition*. John Wiley & Sons Inc: Hoboken, New Jersey, United States of America, 2007.
51. Feinberg J, Langtangen HP. *Chaospy software package for uncertainty quantification*, 2014. (Available from: https://github.com/hplgit/chaospy).
52. Eldred MS, Giunta AA, van Bloemen Waanders BG, Wojtkiewicz SF, Hart WE, Alleva MP. *DAKOTA, a multilevel parallel object-oriented framework for design optimization, parameter estimation, uncertainty quantification, and sensitivity analysis: version 4.1 reference manual*. Sandia National Laboratories Albuquerque, NM, 2007. (Available from: http://dakota.sandia.gov/docs/dakota/4.2/Developers4.2.pdf).
53. Baudin M, Martinez JM. *Nisp toolbox manual, version 0.4*, 2013. (Available from: http://forge.scilab.org/index.php/p/nisp/downloads/566/).
54. Pianosi F, Sarrazin F, Wagener T. A Matlab toolbox for global sensitivity analysis. *Enviromental Modelling & Software* 2015; **70**:80–85.
55. Pujol G, Iooss B, Janon A. *R cran: sensitivity*, 2015. (Available from: http://cran.r-project.org/web/packages/sensitivity/sensitivity.pdf).
56. Buckland ST. Monte Carlo confidence intervals. *Biometrics* 1984; **40**(3):811–817. (Available from: http://www.jstor.org/stable/2530926).
57. Saltelli A. Making best use of model evaluations to compute sensitivity indices. *Computer Physics Communications* 2002; **145**(2):280–297.
58. Saltelli A, Annoni P, Azzini I, Campolongo F, Ratto M, Tarantola S. Variance based sensitivity analysis of model output. Design and estimator for the total sensitivity index. *Computer Physics Communications* 2010; **181**(2):259–270.
59. Jansen MJW. Analysis of variance designs for model output. *Computer Physics Communications* 1999; **117**(1):35–43.
60. Sobol IM, Tarantola S, Gatelli D, Kucherenko SS, Mauntz W. Estimating the approximation error when fixing unessential factors in global sensitivity analysis. *Reliability Engineering and System Safety* 2007; **92**(7):957–960.
61. Herman J. *Sensitivity analysis library in python*, 2015. (Available from: http://jdherman.github.io/SALib/).
62. Wiener N. The homogeneous chaos. *Americal Journal of Mathematics* 1938; **60**(4):897–936.
63. Conrad PR, Marzouk YM. Adaptive smolyak pseudospectral approximations. *SIAM Journal on Scientific Computing* 2013; **35**(6):A2643–A2670. (Available from: https://bitbucket.org/mituq/muq).
64. Électricité de F, company European Aeronautic Defence & Space, Phimeca. *Developer's guide for open TURNS 1.5*, 2007. (Available from: http://doc.openturns.org/openturns-1.5/openturns-doc-february-2015/pdf/OpenTURNS_DevelopersGuide.pdf).
65. Debusschere BJ, Najm HN, Pébay PP, Knio OM, Ghanem RG, Le Maitre OP. Numerical challenges in the use of polynomial chaos representations for stochastic processes. *SIAM Journal on Scientific Computing* 2004; **26**(2):698–719. DOI: 10.1137/S1064827503427741.
66. Eldred MS, Webster CG, Constantine PG. Evaluation of non-Intrusive approaches for Wiener-Askey generalized polynomial chaos. *49th AIAA/ASME/ASCE/AHS/ASC Structures, Structural Dynamics and Materials Conference*, American Institute for Aeronautics and Astronautics, Schaumburg, Illinois, 2008.
67. Blatman G, Sudret B. Sparse polynomial chaos expansions and adaptive stochastic finite elements using a regression approach. *Comptes Rendus Mécanique* 2008; **336**(6):518–523.

68. Blatman G. Adaptive sparse polynomial chaos expansions for uncertainty propagation and sensitivity analysis. *Doctoral Thesis*, 2009.
69. Abramowitz M, Stegun IA. *Handbook of Mathematical Functions*. Dover Publications: New York, 1965.
70. Xiu D. Efficient collocational approach for parametric uncertainty analysis. *Communications in Computational Physics* 2007; **2**(2):293–309.
71. Smolyak SA. Quadrature and interpolation formulas for tensor products of certain classes of functions. *Doklady Akademii Nauk SSSR* 1963; **4**:240–243.
72. Gerstner T, Griebel M. Numerical integration using sparse grids. *Numerical Algorithms* 1998; **18**:209–232.
73. Wasilkowski GW, Wozniakowski H. Explicit cost bounds multivariate tensor product problems. *Journal of Complexity* 1995; **11**:1–56.
74. Petras K. Smolyak cubature of given polynomial degree with few nodes for increasing dimension. *Numerische Mathematik* 2003; **93**:729–753.
75. Donders WP, Huberts W, van de Vosse FN, Delhaas T. Personalization of models with many model parameters: an efficient sensitivity analysis approach. *International Journal for Numerical Methods in Biomedical Engineering* 2015; **31**(5).
76. Hastie T, Tibshirani R, Friedman J. *The Elements of Statistical Learning: Data mining, Inference, and Prediction*. Springer-Verlag: New York, New York, United States of America, 2009.
77. Pijls NHJ, van Gelder B, van der Voort P, Peels K, Bracke Frank ALE, Bonnier HJRM, El G. MIH. Fractional flow reserve: a useful index to evaluate the influence of an epicardial coronary stenosis on myocardial blood flow. *Circulation* 1995; **92**:3183–3193.
78. Tonino PAL, de Bruyne B, Pijls NHJ, Siebert U, Ikeno F, van't Veer M, Klauss V, Manoharan G, Engstrom T, Oldroyd KG, Ver Lee PN, MacCarthy PA, Fearon WF, FAME Study Investigators. Fractional flow reserve versus angiography for guiding percutaneous coronary intervention. *The New England Journal of Medicine* 2009; **360**(3):213–224.
79. Taylor CA, Fonte TA, Min JK. Computational fluid dynamics applied to cardiac computed tomography for noninvasive quantification of fractional flow reservescientific basis. *Journal of the American College of Cardiology* 2013; **61**(22):2233–2241, available at /data/Journals/JAC/927053/11083.pdf. DOI: 10.1016/j.jacc.2012.11.083.
80. Morris PD, Ryan D, Morton AC, Lycett R, Lawford PV, Hose DR, Gunn JP. Virtual fractional flow reserve from coronary angiography: Modeling the significance of coronary lesions. Results from the VIRTU-1 (VIRTUal fractional flow reserve from coronary angiography) study. *JACC: Cardiovascular Interventions* 2013; **6**(2): 149–157.
81. Huo Y, Svendsen M, Choy JS, Zhang ZD, Kassab GS. A validated predictive model of coronary fractional flow reserve. *Journal of The Royal Society Interface* 2012; **9**(71):1325–1338.
82. Glasser SP, Arnett DK, McVeigh GE, Finkelstein SM, Bank AJ, Morgan DJ, Cohn JN. Vascular compliance and cardiovascular disease: a risk factor or a marker? *American Journal of Hypertension* 1997; **10**(10): 1175–1189.
83. Liu ZR, Ting CT, Zhu SX, Yin FC. Aortic compliance in human hypertension. *Hypertension* 1989; **14**(2):129–136. (Available from: http://hyper.ahajournals.org/content/14/2/129).
84. Papaioannou TG, Protogerou AD, Stergiopulos N, Vardoulis O, Stefanadis C, Safar M, Blacher J. Total arterial compliance estimated by a novel method and all-cause mortality in the elderly: the PROTEGER study. *AGE* 2014; **36**(3):1555–1563. DOI: 10.1007/s11357-014-9661-0.
85. Stergiopulos N, Segers P, Westerhof N. Use of pulse pressure method for estimating total arterial compliance in vivo. *American Journal of Physiology - Heart and Circulatory Physiology* 1999; **276**(2):H424–H428.
86. Stergiopulos N, Meister JJ, Westerhof N. Simple and accurate way for estimating total and segmental arterial compliance: the pulse pressure method. *Annals of Biomedical Engineering* 1994; **22**(4):392–397. DOI: 10.1007/BF02368245.
87. Buchanan S, Orris P, Karliner J. Alternatives to the mercury sphygmomanometer. *Journal of Public Health Policy* 2011; **32**(1):107–120.
88. Hunyor SN, Flynn JM, Cochineas C. Comparison of performance of various sphygmomanometers with intra-arterial blood-pressure readings. *BMJ* 1978; **2**(6131):159–162. (Available from: http://www.bmj.com/content/2/6131/159).
89. Chin CWL, Khaw HJ, Luo E, Tan S, White AC, Newby DE, Dweck MR. Echocardiography underestimates stroke volume and aortic valve area: implications for patients with small-area low-gradient aortic stenosis. *Canadian Journal of Cardiology* 2014; **30**(9):1064–1072.
90. Liu ZR, Ting CT, Zhu SX, Yin FC. Aortic compliance in human hypertension. *Hypertension* 1989; **14**(2):129–136. (Available from: http://hyper.ahajournals.org/content/14/2/129).
91. Kucherenko S, Albrecht D, Saltelli A. Comparison of lagin hypercube and quasi Monte Carlo sampling techniques. *Mathematics and Computers in Simulation* 2013.
92. Zuniga MM, Ko J. *Gpc: generalized polynomial chaos*, 2014. (Available from: http://CRAN.R-project.org/package=GPC,R package version 0.1).
93. Morris MD. Factorial sampling plans for preliminary computational experiments. *Technometrics* 1991; **33**(2): 161–174.
94. Campolongo F, Cariboni J, Saltelli A. An effective screening design for sensitivity analysis of large models. *Environmental Modelling & Software* 2007; **22**(10):1509–1518.
95. Blatman G, Sudret B. Efficient computation of global sensitivity indices using sparse polynomial chaos expansions. *Reliability Engineering & System Safety* 2010; **95**(11):1216–1229.

96. Blatman G, Sudret B. Adaptive sparse polynomial chaos expansion based on least angle regression. *Journal of Computational Physics* March 2011; **230**(6):2345–2367.
97. Gerstner T, Griebel M. Dimension–adaptive tensor–product quadrature. *Computing* 2003; **71**(1):65–87. DOI: 10.1007/s00607-003-0015-5.
98. Nobile F, Tempone R, Webster CG. An anisotropic sparse grid stochastic collocation method for partial differential equations with random input data. *SIAM Journal on Numerical Analysis* 2008; **46**(5):2411–2442.
99. Perkó Z, Gilli L, Lathouwers D, Kloosterman JL. Grid and basis adaptive polynomial chaos techniques for sensitivity and uncertainty analysis. *Journal of Computational Physics* 2014; **260**:54–84.
100. Eldred MS. Design under uncertainty employing stochastic expansion methods. *International Journal for Uncertainty Quantification* 2011; **1**(2):119–146.
101. Eldred MS, Swiler LP, Tang G. Mixed aleatory-epistemic uncertainty quantification with stochastic expansions and optimization-based interval estimation. *Reliability Engineering and System Safety* 2011; **96**(9):1092–1113. DOI: 10.1016/j.ress.2010.11.010.
102. Zhang Z, Hu X, Hou TY, Lin G, Yan M. An adaptive ANOVA-based data-driven stochastic method for elliptic PDEs with random coefficient. *Communications in Computational Physics* 2014; **16**(3):571–598.
103. Karagiannis G, Lin G. Selection of polynomial chaos bases via bayesian model uncertainty methods with applications to sparse approximation of PDEs with stochastic inputs. *Journal of Computational Physics* 2014; **259**: 114–134.
104. Saltelli A, Tarantola S, Campolongo F, Ratto M. *Sensitivity Analysis in Practice. A guide to assessing scientific models*. John Wiley & Sons, Ltd: Chichester, United Kingdom, 2004.
105. Kucherenko S, Tarantola S, Annoni P. Estimation of global sensitivity indices for models with dependent variables. *Computer Physics Communications* 2012; **183**(4):937–946. DOI: 10.1016/j.cpc.2011.12.020.
106. Mara TA, Tarantola S. Variance-based sensitivity indices for models with dependent inputs. *Reliability Engineering & System Safety* 2012; **107**:115–121.
107. Chastaing G, Gamboa F, Prieur C. Generalized sobol sensitivity indices for dependent variables: numerical methods. *Journal of Statistical Computation and Simulation* 2015; **85**(7):1306–1333.
108. Nataf A. Détermination des distributions de probabilitées dont les marges sont données. *Comptes rendus de l'academie des sciences* 1962; **225**:42–43.
109. Rosenblatt M. Remarks on a multivariate transformation. *Annals of Mathematical Statistics* 1952; **23**(3):470–472. http://www.jstor.org/stable/2236692.
110. Feinberg J, Langtangen HP. *Multivariate polynomial chaos with dependent variables*, 2015. (Available from: https://github.com/hplgit/chaospy/blob/master/doc/mulitivariate_pce.pdf).
111. Sacks J, Welch WJ, Mitchell TJ, Wynn HP. Design and analysis of computer experiments. *Statistical Science* 1989; **4**(4):409–423. (Available from: http://www.jstor.org/stable/2245858$\delimiter"026E30F$nhttp://www.jstor.org/stable/pdfplus/2245858.pdf?acceptTC=true).
112. Oakley JE, O'Hagan A. Probabilistic sensitivity analysis of complex models: a Bayesian approach. *Journal of the Royal Statistical Society: Series B (Statistical Methodoloty)* 2004; **66**(3):751–769. DOI: 10.1111/j.1467-9868.2004.05304.x/ful l.
113. Melis A, Clayton RH, Marzo A. *A more efficient approach to perform sensitivity anlayisi in 0d/1d cardiovascular models*, 29.06.2015. (Available from: http://www.compbiomed.net/2015/cmbe-proceedings.htm).
114. Koutsourelakis Ps. Accurate uncertainty quantification using inaccurate computational models. *SIAM Journal of Scientific Computing* 2009; **31**(5):3274–3300.
115. Ng LWT, Eldred MS. Multifidelity uncertainty quantification using non-intrusive polynomial chaos and stochastic collocation. *53rd AIAA/ASME/ASCE/AHS/ASC Structures, Structural Dynamics and Materials Conference*, American Institute of Aeronautics and Astronautics, 2012; 1–17.
116. Le Gratiet L, Cannamela C, Iooss B. A Bayesian approach for global sensitivity analysis of (multifidelity) computer codes. *SIAM/ASA Journal of Uncertainty Quantification* 2014; **2**:336–363, available at arXiv:1307.2223v1.